

Research Article

Inhibition of Indoleamine 2,3-Dioxygenase in the Prelimbic and Infralimbic Cortices Exerts Antidepressant Effects through Different Pathways in ICV-STZ Rats

Yu Qin, Xiao Hu, Hui-Ling Zhao, Nurhumar Kurban, Xi Chen, Jing-Kun Yi, Yuan Zhang, Su-Ying Cui* and Yong-He Zhang*

Department of Pharmacology, Peking University, School of Basic Medical Science, Beijing, China

ARTICLE INFO

Article history:

Received: 9 October, 2023

Accepted: 15 November, 2023

Published: 29 December, 2023

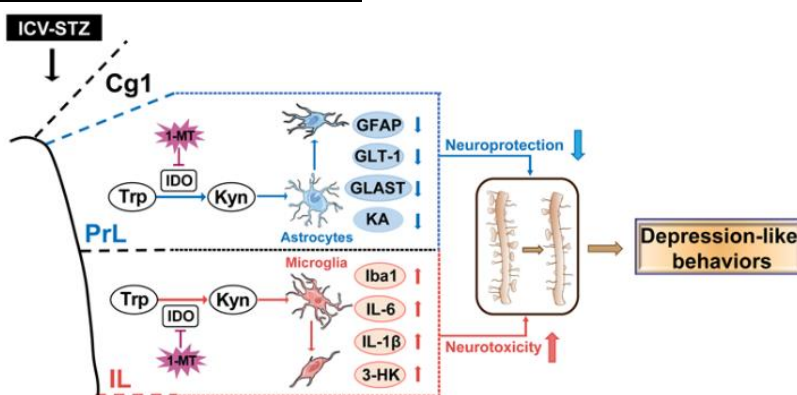
Keywords:

Depression, IDO, prelimbic cortex, infralimbic cortex, astrocyte, microglia

ABSTRACT

An intracerebroventricular injection of streptozotocin (ICV-STZ) is used to simulate sporadic Alzheimer's disease (sAD) in rats. Rats exhibit depression-like behaviors at the beginning of this model. Indoleamine 2,3-dioxygenase (IDO), a rate-limiting enzyme catalyzing the conversion of tryptophan to kynurenine, is closely related to AD and depression. Present study investigated the neurophysiological mechanism of depression-like behaviors in ICV-STZ rats with a focus on IDO-related kynurenine pathways. IDO was activated in both the prelimbic cortex (PrL) and infralimbic cortex (IL), but abnormalities in downstream metabolic pathways were dramatically different and associated with separate secondary biological effects. In the PrL, the neuroprotective branch of the kynurenine pathway was attenuated, as evidenced by a decrease in kynurenic acid and kynurenine aminotransferase II accompanied by defects in astrocytes, reflected by decreases in GFAP-positive cells and glial transporters and morphological damage. In the IL, the neurotoxic branch of the kynurenine pathway was enhanced, as evidenced by an increase in 3-hydroxy-kynurenine and kynurenine 3-monooxygenase paralleled by the overactivation of microglia, reflected by an increase in Iba1-positive cells and cytokines with morphological alterations. Synaptic plasticity was attenuated in both subregions. Additionally, a microinjection of the selective IDO inhibitor 1-MT in the PrL or IL alleviated depression-like behaviors by reversing these different abnormalities in the PrL and IL. These results suggest that the antidepressant effects of IDO inhibition in the PrL and IL occur through different pathways, namely by enhancing neuroprotective effects in the PrL and attenuating neurotoxic responses in the IL.

© 2023 Yong-He Zhang & Su-Ying Cui. Published by Progress in Neurobiology

Graphical Abstract: Qin *et al.* 1-MT improve depression in distinct ways in PrL and IL.*Correspondence to: Dr. Yong-He Zhang, Department of Pharmacology, Peking University, School of Basic Medical Science, Beijing 100191, China; Fax: +861082801112; E-mail: zhyh@hsc.pku.edu.cnDr. Su-Ying Cui, Department of Pharmacology, Peking University, School of Basic Medical Science, Beijing 100191, China; Fax: +861082801112; E-mail: csy@bjmu.edu.cn

© 2023 Yong-He Zhang & Su-Ying Cui. This is an open-access article distributed under the terms of the Creative Commons Attribution License, which permits unrestricted use, distribution, and reproduction in any medium, provided the original author and source are credited. Published by Progress in Neurobiology.

DOI: 10.60124/j.PNEURO.2023.30.05

Highlights

- ICV-STZ induced depressive behavior before cognitive impairment.
- ICV-STZ induced regionally specific pathological changes between PrL and IL.
- Inhibition of IDO in PrL improves depressive behavior via enhancing neuroprotection.
- Inhibition of IDO in IL improves depressive behavior via attenuating neurotoxicity.

1. Introduction

Alzheimer's disease (AD) is a common progressive neurodegenerative disorder characterized by cognitive and behavioral disabilities [1]. Epidemiologically, nearly all AD patients have neuropsychiatric symptoms, the most common of which is depressive mood [2]. Evidence suggests that depression might be a prodromal symptom of AD and seriously reduce quality of life [3, 4], while the pathophysiological mechanisms that underlie depression in AD patients are less well defined. These patients were treated with the conventional antidepressants, but the efficacy is uncertain and even serious adverse effects have been observed [5, 6]. These facts suggest that the pathological mechanisms of depression in AD patients may be different from that of major depressive disorder, and it is necessary to be elucidated.

More than 95% of AD patients have sporadic AD (sAD) [7]. Streptozotocin (STZ), a glucosamine compound with β -cytotoxic action, is commonly used to induce diabetes in laboratory animals [8]. Recently, some investigators exploited the intracerebroventricular micro-injection of STZ (ICV-STZ) to simulate sporadic AD in rodents as a non-transgenic model of this disease and used for preclinical testing of pharmacological therapies for AD [9]. Single or double ICV-STZ injection(s) chronically produce progressive pathological changes that resemble molecular, pathological, and behavioral features of AD [10-12]. Specifically, ICV-STZ induce amyloid- β (A β) accumulation and tau hyperphosphorylation as results of oxidative stress and immunoinflammatory response in cortex and hippocampus, which finally cause learning and cognitive impairments [11, 13]. Furthermore, ICV-STZ also induces noncognitive features of AD, such as depression-like behavioral in rodents [14, 15]. Although the pathophysiological mechanism of depression-like behaviors in STZ-induced AD model is unclear, some pilot researches indicated that the activation of indoleamine-2,3-dioxygenase (IDO) might be a key factor [16].

IDO is a rate-limiting enzyme in the kynurenine pathway that catalyzes the conversion of tryptophan (Trp) to kynurenine (Kyn) [17]. Subsequently, intermediates of Kyn are metabolized into kynurenic acid (KA), which has neuroprotective effects mainly produced by kynurenine aminotransferase (KAT) II located in astrocytes, while Kyn is also metabolized in microglia by kynurenine 3-monooxygenase (KMO) to 3-hydroxykynurenine (3-HK) and quinolinic acid to induce excitotoxic effects [17]. It has been reported that the abnormalities in IDO-related Kyn metabolism occurred in glial play a prominent role in the processes of neuroinflammation [18, 19], and these abnormalities were also found in ICV-STZ animal models. Souza *et al.* [20] reported that ICV-STZ-

associated depression-like behaviors in mice may be attributable to the hippocampal IDO activation in response to the upregulation of innate immune and proinflammatory cytokines. In addition, ICV-STZ caused an acute and persistent neuroinflammatory response, reflected by reactive microgliosis and astrogliosis in the dorsal hippocampus [21] and by the hyperactivation of astrocyte in the prefrontal cortex (PFC) [22]. These results indicated that IDO-related glial alterations in certain brain regions might be involved in the regulation of AD-associated depression. Obviously, multiple anatomical brain locations are associated with cognition and emotion. To figure out the main locations, we detected IDO-related metabolisms in several brain regions when these ICV-STZ rats exhibited depression-like behaviors. It was impressive to show that prelimbic cortex (PrL) and infralimbic cortex (IL) were the most obvious regions where IDO was significantly activated by STZ exposure.

The prelimbic cortex (PrL) and infralimbic cortex (IL) are two major medial PFC (mPFC) areas in rodents that are thought to mediate the control of depression-like behaviors [23]. Although the PrL and IL have similar projection patterns in certain aspects, a growing body of research has revealed that they can be functionally distinguished with regard to mediating various physiological and behavioral processes in rodents, including fear expression and extinction [24], cocaine-seeking [25], anxiety [26], and depression [27]. These findings bolster the fact that exploring the subregional mechanisms of mPFC is important for understanding the physiological and pathological process of neurologic disorders.

Therefore, the present study investigated depression-like behavior and the neurophysiological mechanism of action of IDO on Kyn pathways in the PrL and IL in the rat model of ICV-STZ. We evaluated the effects of ICV-STZ on the Kyn pathway, astrocytes, microglia, and synaptic plasticity in the PrL and IL. Additionally, IDO inhibitor 1-MT was directly injected in the PrL and IL to study its antidepressant-like effect and influence on the above pathological mechanisms.

2. Method

2.1. Animals

Adult male sprague-dawley rats (250-280 g weight) were procured from the Animal Center of Peking University (Beijing, China). All rats were housed individually in plastic cages with ad libitum access to food and water at an optimum temperature of (25 \pm 2) °C and 55%-65% relative humidity. The position of the bottle was in the middle of the cage cover to eliminate location bias. A 12 h/12 h light/dark cycle (lights on at 9:00 AM) was regulated in the animal house. All rats were allowed to acclimate for 7 d before receiving any experimental manipulation. All the experimental procedures were complied with the guidelines of the "Animal Research: Reporting of *In Vivo* Experiments (ARRIVE)" [28] and carried out in accordance with the National Research Council's Guide for the Care and Use of Laboratory Animals. The animal experiment protocol was approved by the Peking University Committee on Animal Care and Use (permission no. LA 2020279).

2.2. Surgery for Cannula Implantation

Rats were anesthetized with isoflurane (5% induction and 2% maintenance) and placed in a stereotaxic frame. A unilateral and a bilateral guide cannula (O.D. 0.64 mm × I.D. 0.25 mm, C.C. 1.2 mm, RWD Life science Co Ltd., Shenzhen, China) were chronically implanted in the lateral ventricle (-0.8 mm AP; -1.5 mm ML; -3.5 mm DV) and mPFC (PrL: +3.2 mm AP; ±0.6 mm ML; -2.6 mm DV, IL: +3.2 mm AP; ±0.6 mm ML; -3.8 mm DV) [29], respectively. The cannula and three anchor screws were bonded to the skull with dental acrylic and dental cement. After surgery, rats were placed on a heated pad and observed for at least 30 min, then returned to its original cage. Rats were handled and checked for signs of pain and distress at least once daily. Topical analgesic (lidocaine/prilocaine cream) was used to prevent signs of pain and/or discomfort for at least 2-3 d. The rats were intramuscularly injected with penicillin (400000 IU/kg) for at least 3 d and allowed to recover for 7 d before the experiments began.

2.3. Drugs and Treatment

The ICV-STZ procedure was used as previously described [30, 31]. After 7 d of recovery from surgery, streptozotocin (Sigma-Aldrich, Cat#

S0130, MO, USA) was administered on d 1 and d 3 at 3:00-5:00 PM at a dose of 3 mg/kg dissolved in (4±1) μL artificial cerebrospinal fluid (aCSF; Tocris Bioscience, Cat# 3525/25 ML, Bristol, UK) according to body weight. Streptozotocin was slowly injected into the lateral ventricle using a hamilton microsyringe fixed to the syringe pump (RWD Life Science Co Ltd., Shenzhen, China) and connected to the injection cannula at a rate of 0.8 μL/min. The needle was left in place for an additional 3 min to allow for diffusion. The vehicle rats were administered with an equal volume of aCSF.

1-Methyl-DL-tryptophan (1-MT; Sigma-Aldrich, Cat# 860646, MO, USA) was dissolved in 1 M HCl and adjusted the pH to 6.5 using NaOH, then diluted using 0.9% sterile sodium chloride solution to the final treatment concentration [32]. 1-MT was injected once daily into the PrL or IL bilaterally (0.2 μL per side) at a rate of 0.1 μL/min at 9:00-11:00 AM from d 1 to d 8. The injection cannula was kept in place for another 2 min to allow the drug to diffuse from the tip entirely. According to O'Connor *et al.*, the effective dose of 1-MT in the brain to produce antidepressant effects is 50 μg/mL [33]. The vehicle rats were administered with an equal volume of 0.9% sterile sodium chloride solution.

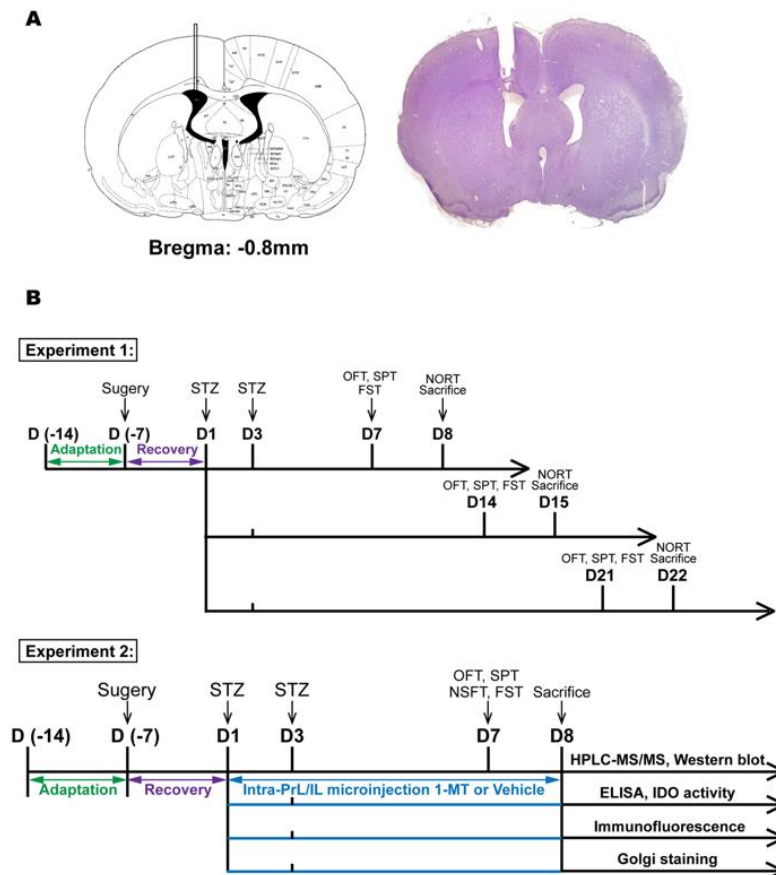


FIGURE 1: A) Location of intracerebroventricular injection sites and B) experimental design.

2.4. Nissl Staining

Nissl staining was used to confirm cannula placement and carried out using a nissl stain kit (Solarbio, Cat# G1430, China). Anesthetized rats

were perfused slowly with 200 mL of 0.01 M phosphate-buffered saline (PBS) and 200 mL of 4% paraformaldehyde. Whole brains were immediately removed, soaked in 4% paraformaldehyde at 4 °C for 24 h, and then successively transferred to 20% sucrose and 30% sucrose at 4

°C until tissues were sunk. The brains were rapidly frozen in liquid optimal cutting temperature compound (Sakura Finetek, Cat# 4583, CA, USA) cooled with a mixture of solid carbon dioxide and ethanol. Serial coronal brain sections were cut into 20 µm thickness on a cryostat microtome (Leica Microsystems UK, Leica CM1950, Milton Keynes, UK) and stored at -20 °C in cryoprotectant solution (48% PBS, 30% ethylene glycol, 20% glycerol, 2% DMSO). Brain sections were stained with reagent A (cresyl violet Stain) for 1 h at 56 °C. Subsequently, the sections were washed with distilled water, immersed in reagent B (nissl differentiation) for seconds to 2 min, and dehydrated in absolute ethanol. Finally, the sections were cleared in xylene before being cover-slipped with neutral balsam (Solarbio, # G8590, China). The image was scanned by a Nikon DS-Ri2 microscope camera (Nikon, Tokyo, Japan) acquired at 1x magnification. The cannula placements of the lateral ventricle are shown in (Figure 1A).

2.5. Experiment Design

The experimental design is presented in (Figure 1B). In the experiment 1, five rats with surgery-related infections were excluded. Then, the rats were randomly grouped into 5 groups (8 animals in each group): i) control: no surgery; ii) vehicle: ICV-aCSF; iii) ICV-STZ 7 d; iv) ICV-STZ 14 d; v) ICV-STZ 21 d. Behavioral tests performed as previously described [34, 35] were conducted on d 7, d 14 and d 21, respectively. The open field test (OFT) was performed at 9:00 AM, the sucrose preference test (SPT) was performed at 12:00 PM. Following break the forced swim test (FST) stated at 4:00 PM. The novel object recognition test (NORT) was performed at 9:00 AM on d 8, d 15 and d 22, respectively. In the experiment 2, rats were randomly grouped into 4 groups (6 animals in each group) in each separate intra-PrL or intra-IL microinjection experiment: i) vehicle (ICV)+vehicle (PrL or IL); ii) vehicle (ICV)+1-MT (PrL or IL); iii) STZ (ICV)+vehicle (PrL or IL); iv) STZ (ICV)+1-MT (PrL or IL). Animal body weight and food consumption were measured daily. The water intake was measured daily from d 1 to d 5 before food and water deprivation. All behavioral tests were conducted on d 7. The OFT was performed at 9:00 AM, the SPT was performed at 12:00 PM, the novelty-suppressed feeding test (NSFT) was performed at 2:00 PM. Then, rats were allowed to eat and drink freely until the FST stated at 4:00 PM. The rats were decapitated on d 8, and the tissue was used for HPLC-MS/MS and western blot. The other three identical and independent experiments (n=6 in each group) were used for ELISA, IDO activity, immunofluorescence staining and golgi staining, respectively.

2.6. Behavioral Assessment

2.6.1. Forced Swim Test

The FST procedure was conducted according to our previous study [34]. On the pretest day, each rat was individually placed for 15 min into a 25 cm diameter × 60 cm high plexiglas cylinder filled with (24±1) °C water to a depth of 40 cm. On the test day, the rat was placed into the same cylinder again and recorded for 5 min. The water was changed between testing sessions. Behavior was recorded by two video cameras (one on top and one on the side). After the experiment, rats were removed from the water, dried with a towel, and returned to their home cage. The videotapes were analysed by a researcher who was blinded to each rat's

treatment condition. Immobility was defined as the minimum movement necessary to keep the rat's head above the water. Increased immobility time indicated a state of helplessness.

2.6.2. Sucrose Preference Test

The SPT was used to determine anhedonia-like behavior, which is considered a core symptom of depression. The SPT was performed according to a modified version of the paradigm [36]. During the training phase, rats were habituated to drinking from two bottles of 1% sucrose for 48 h. After training, the rats were deprived of food and water for 24 h before the test. On the test day, one bottle containing 1% sucrose solution in tap water and the other containing tap water alone were placed in the rat's home cages simultaneously, and rats were allowed to drink freely from both bottles for 1 h. Water and sucrose consumption was measured by comparing the weight difference of the bottles before and after the test. Anhedonia was assessed as sucrose preference, which was calculated according to the following formula: sucrose preference = $\frac{\text{sucrose intake [g]}}{\text{sucrose intake [g]} + \text{water intake [g]}} \times 100\%$. To exclude the non-specific suppression of drinking, total fluid consumption was calculated as the sum of sucrose intake and water intake.

2.6.3. Open Field Test

The OFT was performed to evaluate locomotor activity and anxiety-like behavior. Rats were submitted individually to a plexiglas chamber (40 cm × 40 cm × 65 cm) with white light on the top, and behavior was recorded by an automated video tracking system (DigBehv-LM4, Shanghai Jiliang Software Technology, Shanghai, China). The video files were later analysed using DigBehv analysis software. In 10 min, the total distance is often used as an auxiliary indicator in FST to rule out prolonged immobility time due to reduced locomotor activity. And time in center (20 cm × 20 cm in the center area) is considered an indicator of anxiety-behavior. The apparatus was wiped with 75% alcohol between tests to eliminate any smell.

2.6.4. Novel Object Recognition Test

The NORT is used to evaluate declarative memory and object recognition and has an essential application in the study of cognitive alterations [37]. The test was performed in a plexiglas box described in 2.6.3, and the task procedures consist of three phases: habituation, training, and test. The rats were habituated to the test box for 20 min on the habituation phase (24 h before the training phase, usually an extra 10 min after the OFT). During the training phase, two identical objects were placed in opposite walls of the testing box, and the animals were allowed to explore for 10 min. Then, we changed one object to a different shape and color in the test phase, and a test session of 10 min was performed after a retention interval of either 2 h. The behavior of the subjects in each trial was recorded on video, and the exploration time was scored by an observer blinded to the experimental conditions. Exploration was defined as sniffing, biting, licking or touching the object with the nose. Turning around or sitting on the object was not considered exploratory behavior. During the test session, a discrimination index (DI) was calculated using the formula $(B-A)/(B+A)$, with B being the time spent

exploring the novel object and A being the time spent exploring the familiar object.

2.6.5. Novelty-Suppressed Feeding Test

The NSFT is most widely used to check the efficacy and efficiency of chronic and sub-chronic antidepressant treatments in rodent models and is performed as previously described [38]. The test was performed in an open field containing five to six food pellets placed in the middle of the arena. Rats were deprived of food at least 24 h before the test. After SPT, individual rats were placed in the corner of the round arena (120 cm in diameter) with dim light on the top and allowed to explore it freely for 10 min. The latency for the rat from leaving the corner of the arena to pick up food was recorded. The latency to feed was measured up to 10 min. The increase in latency to feed is considered a measure of anhedonia based on food. After the NSFT, the rats were returned to their home cages and allowed to eat food. Food consumption within 1 h across the groups was recorded to exclude the non-specific ingestive behavior.

2.7. Estimation of Kynurenine Metabolites

The concentrations of serotonin (5-hydroxytryptamin, 5-HT), Trp, Kyn, 3-HK and KA were measured using an HPLC-MS/MS method as described by Han *et al.* [39] with slight modifications. Briefly, tissue was transferred into a new EP tube, then mixed with 90 μ L of prechilled (4 °C) methanol (0.1% formic acid)-aqueous (8:2, v/v) mixture and 10 μ L of IS (2-Cl-Phe; 1 μ g/mL). The mixture was homogenized using an ultrasonic homogenizer followed by centrifugation at 20,000 \times g for 20 min at 4 °C. After centrifugation, the separated supernatant was transferred into a 2 mL auto sampler, and 10 μ L was injected into the system at a flow rate of 0.4 mL/min. The standard curve was prepared using the same procedure as the brain sample. Each data points comes from an individual rat.

The HPLC-MS/MS system consisted of a Dionex UltiMate 3000 ultra-HPLC system (Thermo, San Jose, CA, USA) and an API 4000Q trap mass spectrometer (AB SCIEX, Foster City, USA) equipped with an electrospray ionization (ESI) source interface. The optimized mass spectrometric parameters were set as follows: curtain gas, 15 psi; collision gas, 2; ion spray voltage, 5500 V for positive mode or -4500 V for negative mode; ion source temperature, 600 °C; ion source gas 1, 55 psi; ion source gas 2, 55 psi. Accurate quantification was operated in multiple reaction monitoring (MRM) mode; the transitions were m/z 177.1→160.1 for 5-HT (positive), m/z 205.1→146.1 for Trp (positive), m/z 209.1→94.1 for Kyn (positive), m/z 225.1→208.1 for 3-HK (positive), m/z 188.0→144.0 for KA (negative). The declustering potential (DP) was set at 35, 40, 60, 45 and -40 V, and the collision energy (CE) was 12, 24, 22, 14 and -22 V for 5-HT, Trp, Kyn, 3-HK and KA, respectively.

Chromatographic separation was performed on an ultimate XB-C18 column (100 mm \times 2.1 mm, 5 μ m, Welch Materials, Inc.). Mobile phase A was water containing 0.1% formic acid, and mobile phase B was acetonitrile. The temperature of the auto sampler was set at 4 °C. Gradient separation was set as follows: 0-1 min, 5% B; 1-3 min, 5-60% B; 3.1-5 min, 5% B for column equilibration. The analysis was performed in a total run time of 5 min. Under these conditions, the

retention times were 2.41, 3.53, 1.97, 0.89 and 3.68 min for 5-HT, Trp, Kyn, 3-HK and KA, respectively. The above data were recorded and analysed using AB SCIEX analyst 1.6 software.

5-hydroxytryptamin (5-HT, purity \geq 98%, Cat# H9523), tryptophan (Trp, purity \geq 99.5%, Cat# 93659), kynurenine (Kyn, purity \geq 98%, Cat# K8625), 3-hydroxy-DL-kynurenine (3-HK, purity \geq 98%, Cat# 148776) and kynurenic acid (KA, purity \geq 98%, Cat# K3375) were purchased from sigma-aldrich (St. Louis, MO, USA). 2-Chloro-L-phenylalanine (2-Cl-Phe, purity=98%, Cat# C105993) used as an internal standard (IS) was purchased from Aladdin Inc. (Shanghai, China). HPLC-grade acetonitrile and methanol were obtained from Fisher Chemical (Fisher Scientific, Shanghai, China).

2.8. Evaluation of Enzyme Activity Indoleamine 2,3-Dioxygenase (IDO)

Quantification of IDO activity was measured through indoleamine 2,3-Dioxygenase 1 (IDO1) activity assay kit (Sigma-Aldrich, Cat# MAK356, MO, USA). Tissue was homogenized using a dounce homogenizer in an ice-cold IDO1 assay buffer with protease inhibitor cocktail containing PMSF. The mixture was then incubated on ice for 5 min and centrifuged at 10,000 \times g for 15 min at 4 °C. Collect the supernatant and add reagents or samples into the 96-well plate according to the table. Incubate the plates in the dark at 37 °C for 45 min, followed by adding 50 μ L of fluorogenic developer solution to each well and incubating at 45 °C for 3 h in the dark with gentle shaking, then allow the plates to cool to room temperature for 1 h. Measure the fluorescence in endpoint mode ($\lambda_{\text{ex}}/\text{nm} = 402$ / $\lambda_{\text{em}}/\text{nm} = 488$) in end-point mode.

2.9. Immunofluorescence Staining and Image Analysis

Immunofluorescence staining was performed as described previously [40]. The steps for obtaining brain sections have been described in detail in 2.4. To label the astrocytes and microglia, a multiple-color immunochemistry kit (Absin, Cat# abs50029, China) was used following the manufacturer's instructions. Briefly, the sections were first placed in PBS (3 \times 5 min) to wash out the cryoprotectant solution. Then, they were incubated in cold acetone for 5 min, followed by washing in PBS (3 \times 5 min). The antigen retrieval was conducted in antibody eluent (Absin, Cat# abs994, China) for 40 min at 37 °C. After washing in PBS (3 \times 5 min), the sections were permeabilized with 0.3% triton X-100 (Sigma-Aldrich, Cat# T9284, MO, USA) for 20 min and blocked with 5% donkey serum at room temperature for 40 min. The sections were then incubated with primary antibodies against GFAP (1:500; rabbit mAb, cell signaling technology, Cat# 80788, MA, USA) for 1 h, and rabbit HRP-conjugated secondary antibody was applied and incubated for 1 h. Next, sections were washed in TBST (3 \times 5 min) and incubated with tyramide signal amplification (TSA) reagent for 10 min. Repeat the above operation and incubated with primary antibodies against Iba-1 (1:500; Rabbit mAb, Cell Signaling Technology, Cat# 17198, MA, USA). Finally, nuclei were subsequently stained with DAPI.

The single images from the PrL and IL for each rat were scanned by a leica TCS-SP8 STED 3X laser scanning confocal microscope (Leica, Germany). Z stacks were performed with 1 μ m steps in the z-direction, and recorded with 1024 \times 1024 pixel resolution in the x-y direction.

Three-dimensional reconstruction of astrocytes and microglia was analysed using imaris software Version 9.0.0 (Bitplane, Concord, MA). The morphological changes in microglia were evaluated following a previously published protocol [41] with modification. Briefly, create a new surface and set the parameters to smooth=0.1, threshold=50 and filter (number of voxels) =20. In edit mode, select 8-10 glial cells with regular and clear shape in whole image field. Then, the surface area and sholl intersection number of GFAP⁺ cells, and terminal points and soma volume of Iba1⁺ cells were examined in statistics tab. Sholl analysis was done by drawing concentric circles as a step by 5 μm , and the number of intersections between the circles and microglia branches was counted, as shown in (Supplementary Figure S1A). These morphological parameters of astrocytes and microglia can reflect complexity and distinguish the state of glia.

2.10. Western Blot

After the rats were decapitated, the brains were immediately removed to a prechilled brain matrix with a 1.0 mm coronal slice thickness (RWD Life Technology, Shenzhen, China). PrL and IL tissues were harvested on ice guided by the Paxinos and Watson rat brain atlas [29] and stored separately in prechilled microcentrifuge tubes at -80 °C until assayed. The tissue was homogenized in RIPA buffer (Solarbio, Cat# R0010, China) supplemented with protease inhibitors (Solarbio, Cat# P0100, China) and phosphatase inhibitors (Solarbio, Cat# P1260, China). Protein (45 μg) was separated by 10% sodium dodecyl sulfate-polyacrylamide gel electrophoresis and transferred to polyvinylidene fluoride (PVDF) membranes (0.45 μm , Millipore, USA). The membranes were blocked with 5% skim milk for 1 h at room temperature and incubated with primary antibodies, including anti- β -actin (1:4000; Rabbit mAb, ABclonal, Cat# AC038, Wuhan, China), anti- β -Amyloid (A β) (1:50; Mouse mAb, Santa Cruz Biotechnology, Cat# sc-28365, CA, USA), anti-tau (1:1000; Mouse mAb, Cell Signaling Technology, Cat# 4019, MA, USA), anti-phospho-tau (Ser199) (1:1000; Mouse mAb, Cell Signaling Technology, Cat# 29957, MA, USA), anti-IDO (1:1000; Rabbit mAb, Cell Signaling Technology, Cat# 86630, MA, USA), anti-KAT II (1:1000; Mouse pAb, Abcam, Cat# ab89608, Cambridge, UK), anti-KMO (1:1000; Rabbit mAb, Abcam, Cat# ab233529, Cambridge, UK), anti-gliial fibrillary acidic protein (GFAP) (1:1000; Rabbit mAb, Cell Signaling Technology, Cat# 80788, MA, USA), anti-glutamate-aspartate transporter (GLAST) (EAAT-1 in humans, 1:1000; Rabbit mAb, cell signaling technology, Cat# 5684, MA, USA), anti-glutamate transporter-1 (GLT-1) (EAAT-2 in human, 1:500; Rabbit pAb, Abcam, Cat# ab41621, Cambridge, UK), anti-ionized calcium-binding adaptor molecule-1 (Iba1) (1:1000; Rabbit mAb, cell signaling technology, Cat# 17198, MA, USA) and anti-BDNF (1:500; Rabbit mAb, Abcam, Cat# ab108319, Cambridge, UK) in TBST buffer (tris-buffered saline + 0.1% Tween-20) overnight at 4 °C. The blots were then washed with TBST three times before incubation with HRP goat anti-mouse IgG (H+L) antibody (1:2000; ABclonal, Cat# AS003, Wuhan, China) or HRP goat anti-rabbit IgG (H+L) antibody (1:2000; ABclonal, Cat# AS014, Wuhan, China) for 2 h at room temperature. After 3 \times 5 min TBST washes, an ecl enhanced kit (ABclonal, Cat# RM00021, Wuhan, China) was used for detection enhancement, and blots were visualized using imageJ software. Each data points comes from an individual rat. The results were normalized to the protein expression level of β -actin.

2.11. Enzyme-Linked Immunosorbent Assay (ELISA)

Rat ELISA kits were used to measure the levels of interleukin-1 β (IL-1 β) (ABclonal, Cat# RK00009, Wuhan, China), interleukin-6 (IL-6) (ABclonal, Cat# RK00020, Wuhan, China) and tumor necrosis factor alpha (TNF- α) (ABclonal, Cat# RK00029, Wuhan, China) in the PrL and IL. Briefly, the tissue was homogenized and centrifuged at 2000 \times g for 20 min at 4 °C, then the supernatant was extracted and incubated in a 96-well plate. The cytokine levels were estimated by interpolation from a standard curve by colorimetric measurements at 450 nm (correction wavelength 630 nm) on an ELISA plate reader (Thermo Fisher Scientific Multiskan Mk3, MA, USA). Each data points comes from an individual rat. The results are shown as pg/mg of protein.

2.12. Golgi Staining

The FD rapid golgi-staining kit (FD NeuroTechnologies, Cat# PK401, Columbia, MD, USA) was used to reveal the density of dendritic spines in pyramidal neurons in the PrL and IL. Brains were immersed in golgi-staining impregnation solution for 2 weeks. Sections were cut at 150 μm on a cryostat at -20 °C to -22 °C. The spines on secondary or tertiary dendrites of pyramidal neurons were calculated at a dendritic segment length of approximately 50 μm . At least 3 dendrites per rat were traced, and a total of 6 rats per group were counted. The images were captured under Nikon Eclipse Ci-L microscope (Nikon, Tokyo, Japan) using DP controller software with 100 \times A/1.25 oil immersion lens. The density of dendritic spines and the dendritic spine morphologies in the PrL and IL were analysed using imageJ software. Dendritic spine density was calculated as the total number of spines per 10 μm length of branch. Dendritic spine morphologies were classified into 4 main types: thin, filopodia, mushroom and stubby [42]. The thin type has a narrow neck with elongated protrusion; the filopodia type was identified as long, thin structures; the mushroom type has a large irregular head with a neck diameter smaller than the head diameter; the stubby type has no obvious constriction between the protrusion and attachment to the neck. The proportion of each type was quantified as ([spine number with each type/total spine number] \times 100).

2.13. Data and Statistical Analysis

The sample size was the number of independent values, and statistical analysis was performed using these independent values. The sample sizes are indicated in the figure legends. The data from western blot were normalized to control group values and determined as 'fold change' in figures. Statistical analysis of the results was done with the help of GraphPad Prism software (version 8; GraphPad Software, Inc., CA, USA). Statistical analysis was undertaken only for studies where each group size was at least n=6. The data are presented as the means \pm SEM. All statistical tests were two-tailed. Unpaired t-test was used to test western blot data and HPLC-MS/MS for vehicle and ICV-STZ 7 d rats of variance. One-way and two-way analysis of variance (ANOVA) followed by tukey's multiple comparison test was applied for comparison among several groups. For two-way ANOVA, the procedure (vehicle or ICV-STZ) and the treatment (saline or 1-MT) were taken as between-group factors. P<0.05 was considered statistically significant in all tests. The experimenter or observer was blind to the groups while analysing the results.

3 Results

3.1. ICV-STZ Induced Depression- and Anxiety-Like Behaviors Before Cognitive Impairment

ICV-STZ rats exhibited a significant increase in immobility time in the FST on d 7 and 14 compared with vehicle rats, indicating depression-like behavior in these rats (Figure 2A). Compared with vehicle rats, immobility time in ICV-STZ rats was not significantly different on d 21 (Figure 2A). In the SPT, ICV-STZ rats exhibited a significant decrease in sucrose preference on d 7 and 14, indicating anhedonia-like behavior (Figure 2B). In contrast, sucrose preference on d 21 was not significantly different from vehicle treatment (Figure 2B). Furthermore, ICV-STZ

rats exhibited a significant decrease in the time spent in the center of the OFT on d 7, 14, and 21, indicating anxiety-like behavior (Figure 2C, E). The total distance travelled in the OFT, representing a measure of locomotor activity, was not significantly different among groups (Figure 2D, E). In the NORT, the exploration time for novel objects significantly increased in control, vehicle, and ICV-STZ 7 d rats, but only a modest, non-significant increase in ICV-STZ 14 d and ICV-STZ 21 d rats (Figure 2F). Also, the discrimination ratio was not significantly different between ICV-STZ 7 d rats and vehicle rats, whereas ICV-STZ 14 d and 21 d rats exhibited a significant decrease in the discrimination ratio compared with vehicle rats (Figure 2F). The result from NORT reflected impairments in recognition memory and discrimination ability were only observed in ICV-STZ 14 d and 21 d rats.

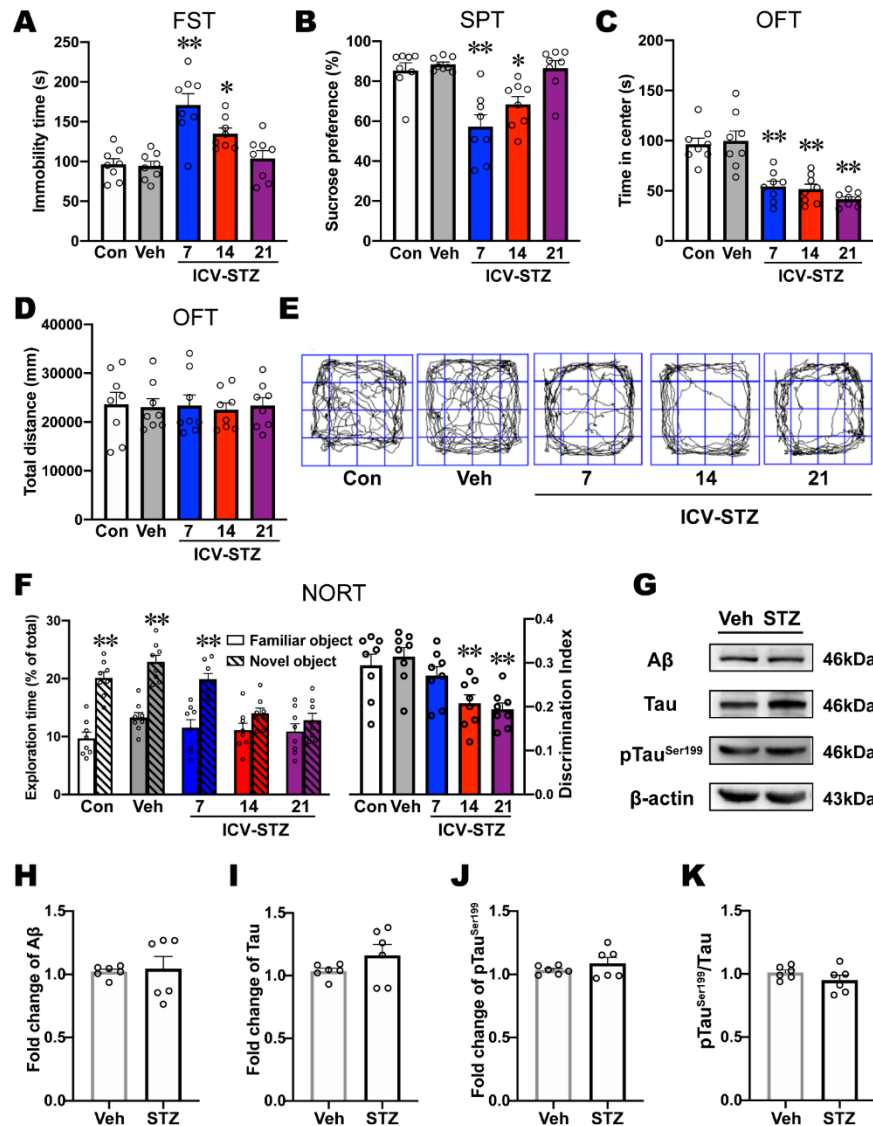


FIGURE 2: ICV-STZ induced depression-like behaviors before cognitive impairment. **A)** Immobility time in the FST and **B)** sucrose preference in the SPT were used to evaluate depression-like behaviors. **C)** The time spent in the center of the OFT was used to evaluate anxiety-like behavior. **D)** The total distance travelled in the OFT was used to detect locomotor activity. **E)** Footprint pattern in the OFT. **F)** Exploration time and the discrimination ratio in the NORT were used to detect recognition memory and discrimination ability ($n = 8$). **G-K)** Western blots and quantification of A β , tau, ptau^{Ser199} protein levels and the ptau^{Ser199}/tau ratio in the mPFC. β -actin was used as the quantitative loading control ($n = 6$). The data are expressed as individual values with means \pm SEM. * $p < 0.05$, ** $p < 0.01$ vs vehicle group; A-F, one-way ANOVA followed by tukey's multiple-comparison post hoc test; H-K, unpaired Student's t -test.

Next, we examined levels of AD-related proteins in the mPFC in ICV-STZ 7 d rats. No significant differences in the expression of A β , tau, or ptau^{ser199} or the ptau^{ser199}/tau ratio were found in the mPFC in ICV-STZ rats, suggesting that AD-related pathological changes were not predominant in the mPFC on d 7 after ICV-STZ treatment (Figures 2G-2K). These results indicated that ICV-STZ induced depression- and anxiety-like behaviors before the expression of cognitive impairment, and as cognition progressively deteriorated, depression-like behavior in ICV-STZ rats gradually disappeared.

3.2. ICV-STZ Induced IDO Activation in PrL and IL

To investigate whether ICV-STZ induced depression-like behaviors are related to the IDO-mediated kynurenine pathway, we examined the levels of kynurenine metabolites in several brain regions associated with mood disorders, including anterior cingulate cortex (ACC), PrL, IL, lateral habenula (LHb), dorsal raphe nucleus (DRN), hippocampus (Hip) and locus coeruleus (LC). ICV-STZ significantly increased Kyn/Trp ratio in the PrL and IL (Figure 3A), which indicated IDO activity was elevated in these two brain regions when these rats exhibited depression-like behaviors.

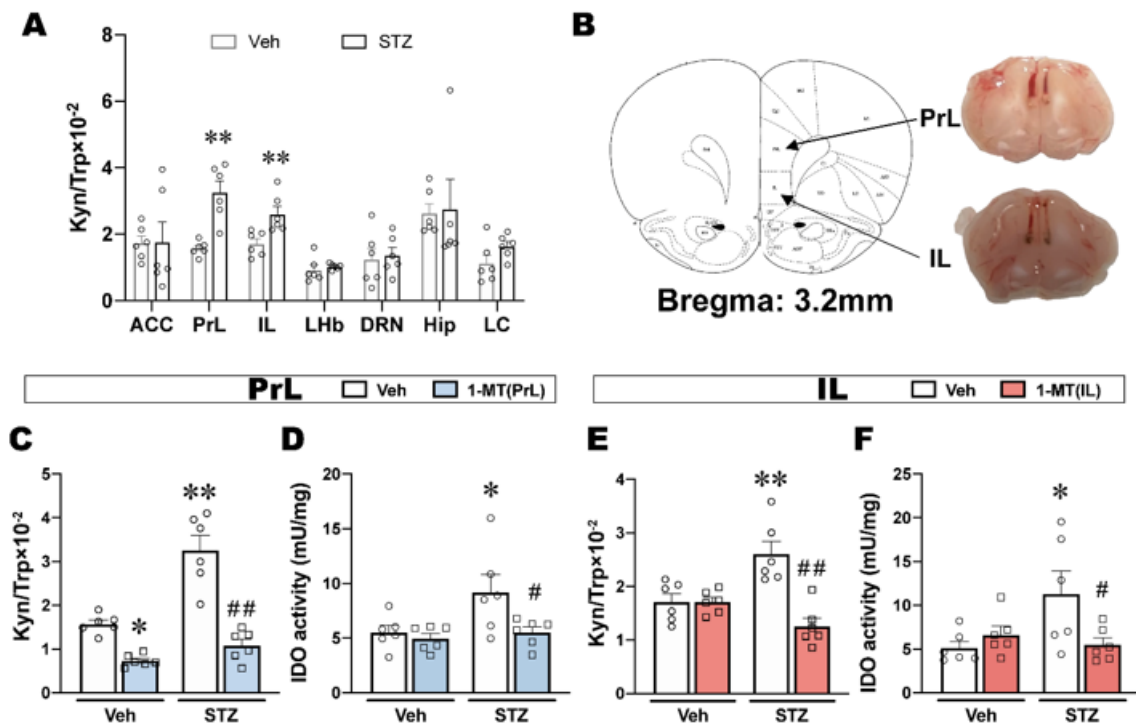


FIGURE 3: ICV-STZ induced IDO activation in PrL and IL. **A)** The Kyn/Trp ratio in several brain regions of ICV-STZ depressed rats ($n = 6$). **B)** Location of PrL and IL injection sites. **C, D)** The Kyn/Trp ratio and IDO activity in the PrL ($n = 6$). **E, F)** The Kyn/Trp ratio and IDO activity in the IL ($n = 6$). The data are expressed as individual values with means \pm SEM. * $p < 0.05$, ** $p < 0.01$ vs vehicle group; # $p < 0.05$, ## $p < 0.01$ vs ICV-STZ group; A, unpaired Student's *t*-test; C-F, two-way ANOVA followed by tukey's multiple-comparison post hoc test.

Next, to directly evaluate whether the activation of IDO in the PrL and IL is responsible for depression-like behavior in ICV-STZ rats, we subsequently inhibited IDO by microinjecting 1-MT in the PrL or IL and observed its effects on the behaviors in ICV-STZ rats. Cannula placements in the PrL and IL are shown in (Figure 3B). There were no significant differences in body weights, food consumption and water intake for all groups until the end of the experiment, suggesting that ICV-STZ and 1-MT treatment had no effect on energy intake and metabolism (Supplementary Figures S2A-S2C). The intra-PrL or intra-IL injection of 1-MT significantly decreased the up-regulation of Kyn/Trp ratio that were induced by ICV-STZ (Figures 3C & 3E). Although ICV-STZ did not cause significant changes in the expression of IDO in the PrL and IL (Supplementary Figures S3A, S3B, S3D & S3E), IDO activity was significantly increased and reversed by intra-PrL or intra-IL injection of 1-MT (Figures 3D & 3F). Furthermore, the levels of 5-HT in both PrL

and IL were not significantly altered in response to ICV-STZ and 1-MT (Supplementary Figures S3C & S3F).

3.3. Intra-PrL/-IL Injection of 1-MT Blocks ICV-STZ-Induced Depression-Like Behaviors

Depression-like behavior that was induced by ICV-STZ, including an increase in immobility time in the FST, a decrease in sucrose preference in the SPT, and an increase in the latency to feed in the NSFT, were reversed by intra-PrL injections of 1-MT (Figures 4A-4C). Food consumption in the NSFT was not significantly different among groups excluded the ingestion bias (Figure 4D). The reduction of time in the center of the OFT was not reversed by 1-MT, and the total distance travelled in the open field was not significantly different among groups (Figures 4E & 4F).

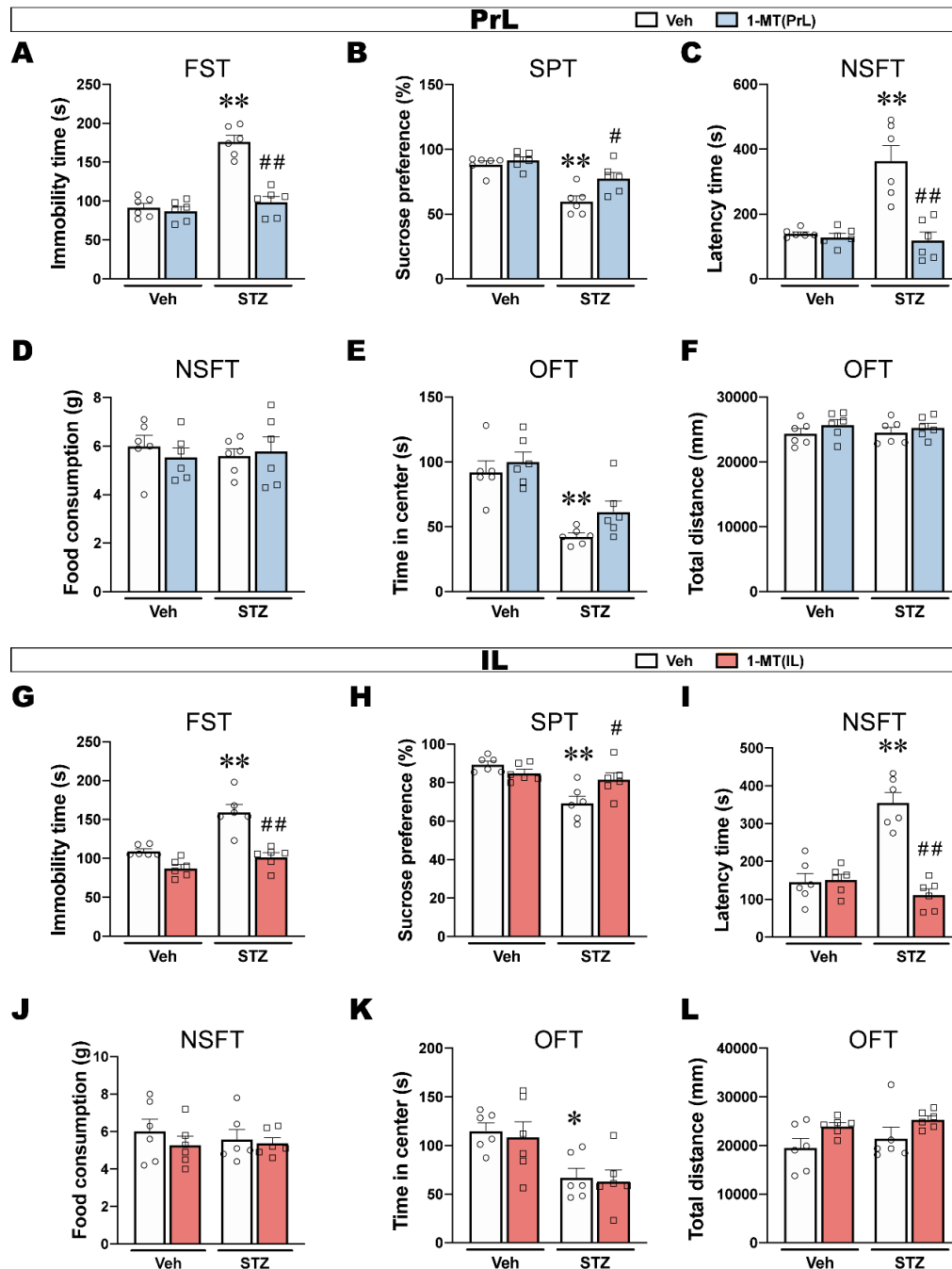


FIGURE 4: Intra-PrL or IL administration of 1-MT prevented depression-like behaviors induced by ICV-STZ. **A, G)** The immobility time in the FST. **B, H)** The sucrose preference in the SPT. **C, I)** The latency time in the NSFT. **D, J)** The food consumption in the NSFT. **E, K)** The time spent in the center of the OFT. **F, L)** The total distance travelled in the OFT (n = 6). The data are expressed as individual values with means ± SEM. **p* < 0.05, ***p* < 0.01 vs vehicle group; #*p* < 0.05, ##*p* < 0.01 vs ICV-STZ group; two-way ANOVA followed by tukey’s multiple-comparison post hoc test.

Similarly, intra-IL injections of 1-MT reversed ICV-STZ-induced depression-like behaviors such as prolonged immobility time, reduced sucrose preference and increased the latency to feed (Figures 4G-4I). In addition, the time in the center of the OFT showed that the intra-IL injections of 1-MT did not reverse anxiety-like behavior in ICV-STZ rats and had no effect on locomotor activity (Figures 4J and 4K).

These results indicated that ICV-STZ induced depression-like behaviors that were likely related to the activation of IDO in the PrL and IL, and both the intra-PrL and intra-IL injections of 1-MT prevented depression-like behavior in ICV-STZ rats. Additionally, the regionally selective blockade of IDO by 1-MT either in the PrL or IL failed to produce an anxiolytic effect, suggesting that anxiety-like behaviors that are induced by ICV-STZ might not be attributable to IDO activation in the PrL and IL, which needs further confirmation.

3.4. ICV-STZ Attenuate Astrocyte Number and Function in the PrL

The kynurenine pathway is regulated by glial cells in the brain. We detected the morphological and functional features of astrocytes and

microglia in the PrL and IL to examine the potential antidepressant mechanism of 1-MT. GFAP was used as an astrocyte marker. Iba1 was used as a microglia marker. The results from PrL and IL are shown in (Figures 5 & 6) separately.

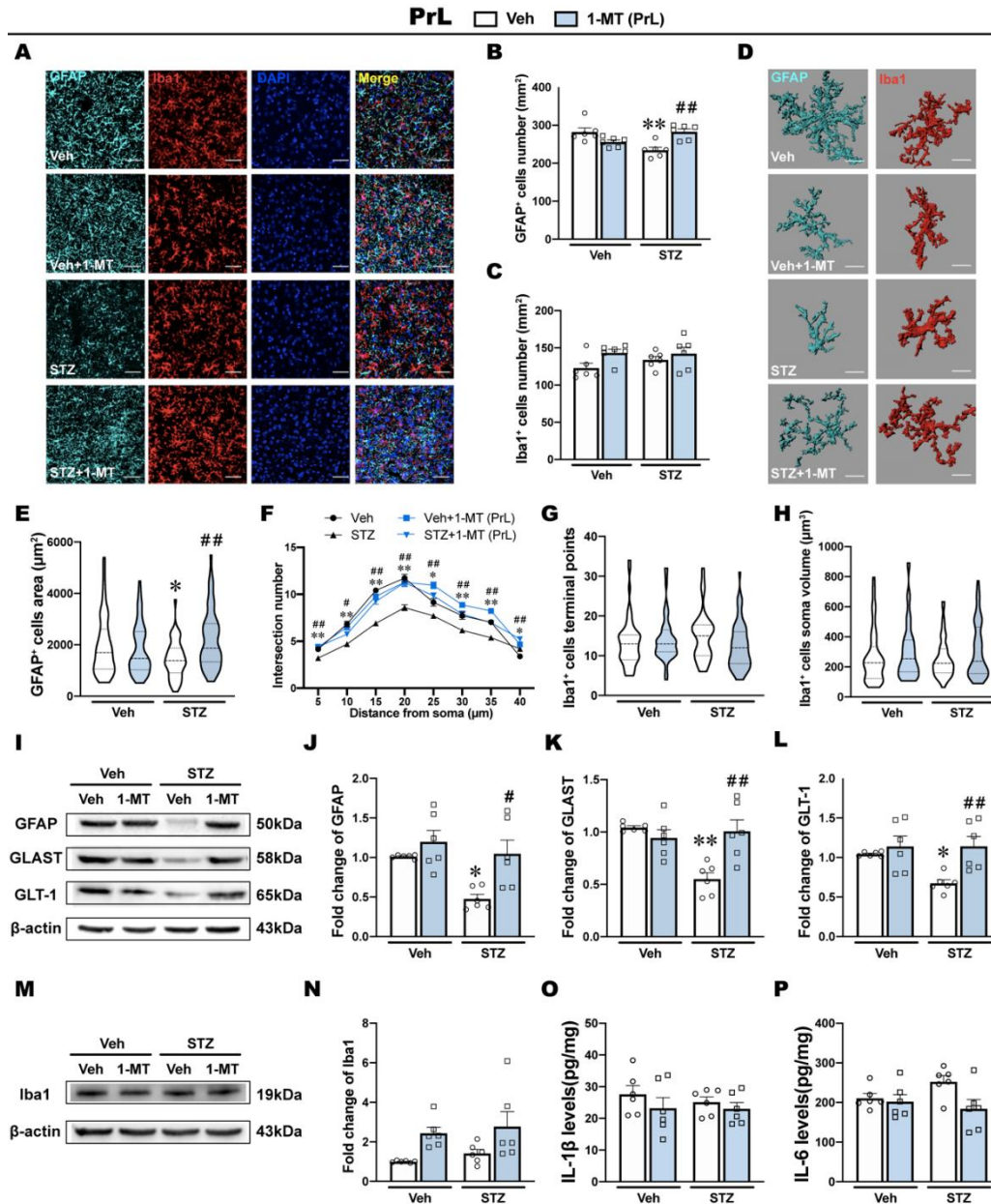


FIGURE 5: ICV-STZ induced astrocyte defects in the PrL, which were reversed by the intra-PrL administration of 1-MT. **A)** Fluorescent images of immunostaining of GFAP and Iba1. GFAP was labeled with TSA monochrome fluorescent dye 570 (cyan). Iba1 was labeled with TSA monochrome fluorescent dye 700 (red). The cell nucleus was counterstained with DAPI (blue). Scale bars = 50 μm. **B)** Counts of GFAP⁺ cells were used to evaluate the expression of astrocytes in the PrL ($n = 6$ slides from 6 rats). **C)** Counts of Iba1⁺ cells were used to evaluate the expression of microglia in the PrL ($n = 6$ slides from 6 rats). **D)** Three-dimensional reconstruction of astrocytes and microglia. Scale bars = 15 μm. **E)** The GFAP⁺ cell area was used to evaluate morphological alterations in the PrL. **F)** Line plot of sholl analysis revealed the number of intersections per 5 μm of astrocytes in the PrL. $n_1 = 58, n_2 = 61, n_3 = 52, n_4 = 65$. **G, H)** The number of Iba1⁺ cell terminal points and soma volume were used to evaluate the state of microglia in the PrL. $n_1 = 60, n_2 = 57, n_3 = 59, n_4 = 61$. **I-L)** Western blots and quantification of GFAP, GLAST, and GLT-1 in the PrL. **M, N)** Western blots and quantification of Iba1 in the PrL. β -actin was used as a quantitative loading control ($n = 6$). **O, P)** Levels of IL-1 β and IL-6 determined by ELISA in the PrL ($n = 6$). The data are expressed as individual values with means \pm SEM. * $p < 0.05$, ** $p < 0.01$ vs vehicle group; # $p < 0.05$, ## $p < 0.01$ vs ICV-STZ group; two-way ANOVA followed by tukey's multiple-comparison post hoc test.

ICV-STZ significantly reduced the number of GFAP⁺ cells in the PrL, which was reversed by the intra-PrL injection of 1-MT (Figures 5A & 5B). However, no significant difference was found in the number of Iba1⁺ cells in the PrL in ICV-STZ rats that were treated with saline or 1-MT (Figures 5A & 5C). Then, we further analyzed the morphological features of glia by performing three-dimensional reconstruction (Figure 5D). Consistent with the above results, the morphological analysis showed a decrease in the surface area of GFAP⁺ cells and sholl analysis showed a lower number of intersections among 5 μm to 40 μm, suggesting the atrophy of astrocytes in the PrL in ICV-STZ rats (Figures 5E & 5F). Intra-PrL injection of 1-MT reversed these morphological abnormalities that were induced by ICV-STZ. Additionally, microglial morphology including terminal points of Iba1⁺ cells and the soma volume of Iba1⁺ cells in the PrL, was not affected by either ICV-STZ or 1-MT (Figures 5G & 5H).

Next, we examined the expression of glia-related proteins and inflammatory cytokines. The western blot analysis showed that ICV-STZ markedly decreased the expression of GFAP in the PrL, accompanied by reductions of GLAST and GLT-1, which are important

components of astrocyte function in glutamate transports (Figures 5I-5L). These defects were restored by the intra-PrL injection of 1-MT, suggesting that the antidepressant effects of 1-MT in ICV-STZ rats might be attributable to protective effects on astrocytes (Figures 5I-5L). On the other hand, the expression of Iba1 in the PrL were not influenced by either ICV-STZ or 1-MT treatment (Figures 5M & 5N). Inflammatory cytokines, including IL-6, IL-1β and TNF- are secreted by microglia within the brain in response to injury and infection. In the PrL, levels of IL-1β, IL-6 and TNF-α were not influenced by either ICV-STZ or 1-MT treatment (Figure 5O, P; Supplementary Figure S4A).

3.5. ICV-STZ Induces Microglia Activation and Inflammatory Response in the IL

In the IL, ICV-STZ and the intra-IL injection of 1-MT had no effect on the number of GFAP⁺ cells per unit area (Figures 6A & 6B). Conversely, the number of Iba1⁺ cells in the IL was significantly increased by ICV-STZ, whereas the intra-IL injection of 1-MT recovered the density of Iba1⁺ cells to normal (Figures 6A & 6C).

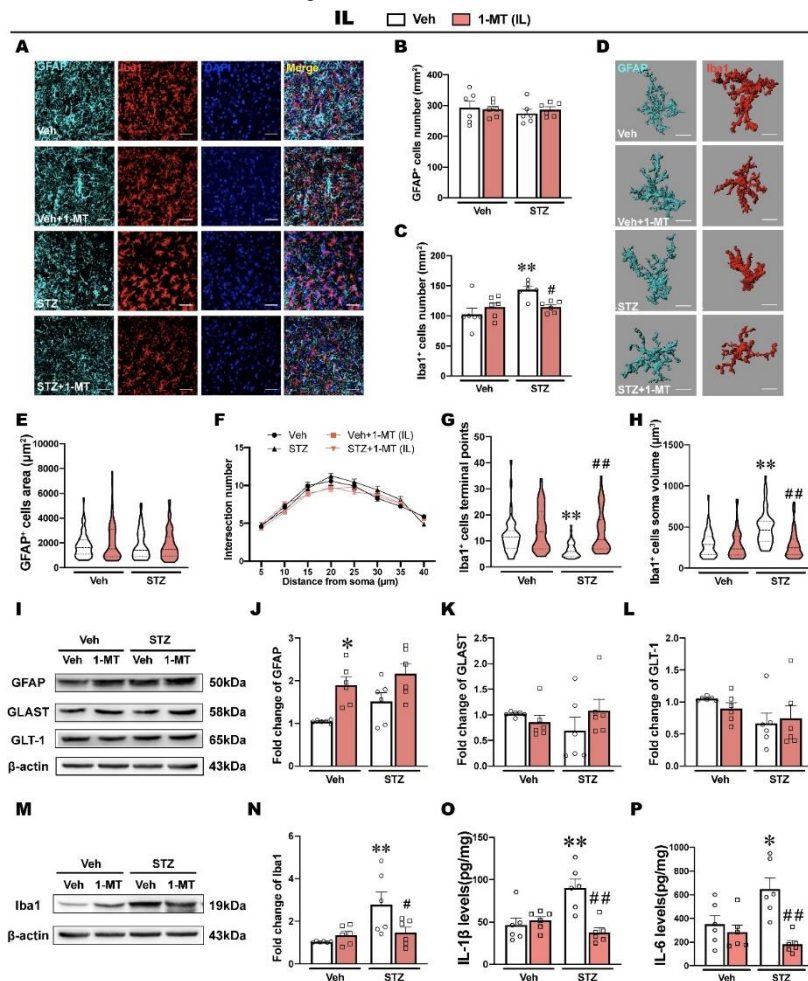


FIGURE 6: ICV-STZ induced microglia overactivation in the IL, which were reversed by the intra-IL administration of 1-MT. **A)** Fluorescent images of immunostaining of GFAP and Iba1. GFAP was labeled with TSA monochrome fluorescent dye 570 (cyan). Iba1 was labeled with TSA monochrome fluorescent dye 700 (red). The cell nucleus was counterstained with DAPI (blue). Scale bars = 50 μm. **B)** Counts of GFAP⁺ cells were used to evaluate the expression of astrocytes in the IL (*n* = 6 slides from 6 rats). **C)** Counts of Iba1⁺ cells were used to evaluate the expression of microglia in the IL (*n* = 6 slides from 6 rats). **D)** Three-dimensional reconstruction of astrocytes and microglia. Scale bars = 15 μm. **E)** The GFAP⁺ cell area was used to evaluate

morphological alterations in the IL. **F**) Line plot of sholl analysis revealed the number of intersections per 5 μm of astrocytes in the IL. $n_1 = 65, n_2 = 64, n_3 = 57, n_4 = 58$. **G, H**) The number of Iba1⁺ cell terminal points and soma volume were used to evaluate the state of microglia in the IL. $n_1 = 48, n_2 = 54, n_3 = 61, n_4 = 48$. (I-L) Western blots and quantification of GFAP, GLAST, and GLT-1 in the IL. **M, N**) Western blots and quantification of Iba1 in the IL. β-actin was used as a quantitative loading control ($n = 6$). **O, P**) Levels of IL-1β and IL-6 determined by ELISA in the IL ($n = 6$). The data are expressed as individual values with means ± SEM. * $p < 0.05$, ** $p < 0.01$ vs vehicle group; # $p < 0.05$, ## $p < 0.01$ vs ICV-STZ group; two-way ANOVA followed by tukey's multiple-comparison post hoc test.

Morphological characterization of the astrocytes in the IL showed that the area of GFAP⁺ cells did not differ significantly among groups, and sholl analysis also showed that the number of intersections was not significantly different among groups (Figures 6D-6F). In contrast, the analysis of morphological features in microglia showed that ICV-STZ significantly decreased terminal points and increased the soma volume of Iba1⁺ cells in the IL, which are typical morphological features of microglia activation [43, 44] (Figures 6G & 6H). The intra-IL injection of 1-MT prevented these morphological abnormalities of microglia induced by ICV-STZ (Figures 6G & 6H).

The western blot analysis showed that ICV-STZ had no effects on the expression of GFAP, whereas 1-MT significantly increased GFAP expression in the IL (Figures 6I & 6J), and there were no significant differences in the expression of GLAST or GLT-1 among groups (Figures 6K & 6L). The expression of Iba1 in the IL was significantly increased by ICV-STZ, and this increase was reversed by the intra-IL injection of 1-MT (Figures 6M & 6N). Correspondingly, levels of IL-1β and IL-6 in the IL significantly increased in ICV-STZ rats, and the intra-IL injection of 1-MT prevented this inflammatory response, which might be associated with its antidepressant effect (Figures 6O & 6P). However, levels of TNF-α in the IL were not influenced by either ICV-STZ or 1-MT treatment (Supplementary Figure S4B).

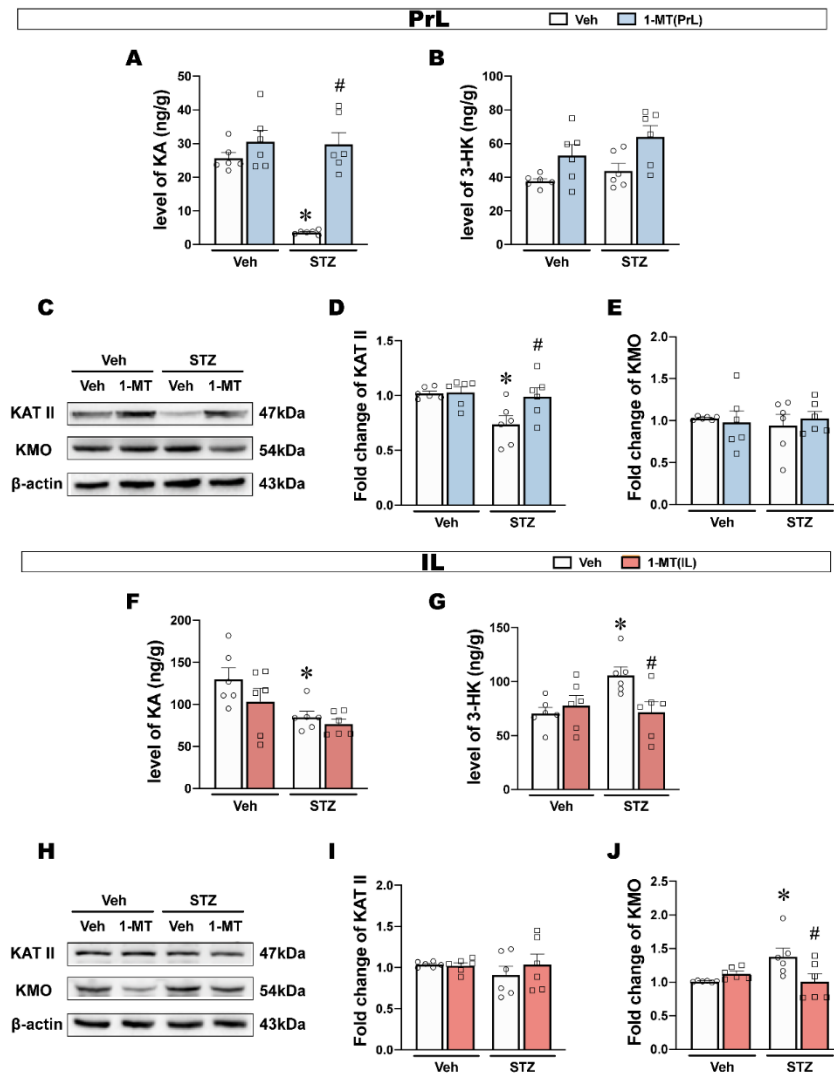


FIGURE 7: ICV-STZ has different effects on the Kyn pathway branches in PrL and IL. **A, B**) Levels of KA and 3-HK in the PrL ($n = 6$). **C-E**) Western blots and quantification of KAT II and KMO in the PrL. β-actin was used as a quantitative loading control ($n = 6$). **F, G**) Levels of KA and 3-HK in the IL ($n = 6$). **H-J**) Western blots and quantification of KAT II and KMO in the IL. β-actin was used as a quantitative loading control ($n = 6$). The data are expressed as

individual values with means ± SEM. * $p < 0.05$, ** $p < 0.01$ vs vehicle group; # $p < 0.05$, ## $p < 0.01$ vs ICV-STZ group; two-way ANOVA followed by tukey's multiple-comparison post hoc test.

3.6. ICV-STZ has Different Effects on the Kyn Pathway Branches in PrL and IL

Kyn and several downstream metabolites have been proposed to be highly correlated with depression [45]. The Kyn pathway branches have been suggested to be separately regulated by microglia and astrocytes, so we next examined Kyn downstream metabolites in both PrL and IL. In the PrL, KA significantly decreased in ICV-STZ rats, and this decrease was reversed by the intra-PrL injection of 1-MT (Figure 7A). However, 3-HK in the PrL were not significantly different among groups (Figure 7B). Furthermore, the KAT II expression in the PrL in ICV-STZ rats was significantly reduced and reversed by 1-MT, while the KMO expression was not significantly changed (Figures 7C-7E).

In the IL, KA levels decreased, but were not reversed by the intra-IL injection of 1-MT (Figure 7F). 3-HK significantly increased, and this increase was reversed by the intra-IL injection of 1-MT (Figure 7G). There was no difference in KAT II expression in the IL of ICV-STZ rats, while KMO expression was significantly increased and reversed by 1-MT (Figures 7H-7J).

These results showed that ICV-STZ exerted different effects on the Kyn metabolic branches in the PrL and IL subregions respectively, mainly in the form of attenuated Kyn-KA branches in the PrL and enhanced Kyn-3-HK branches in the IL.

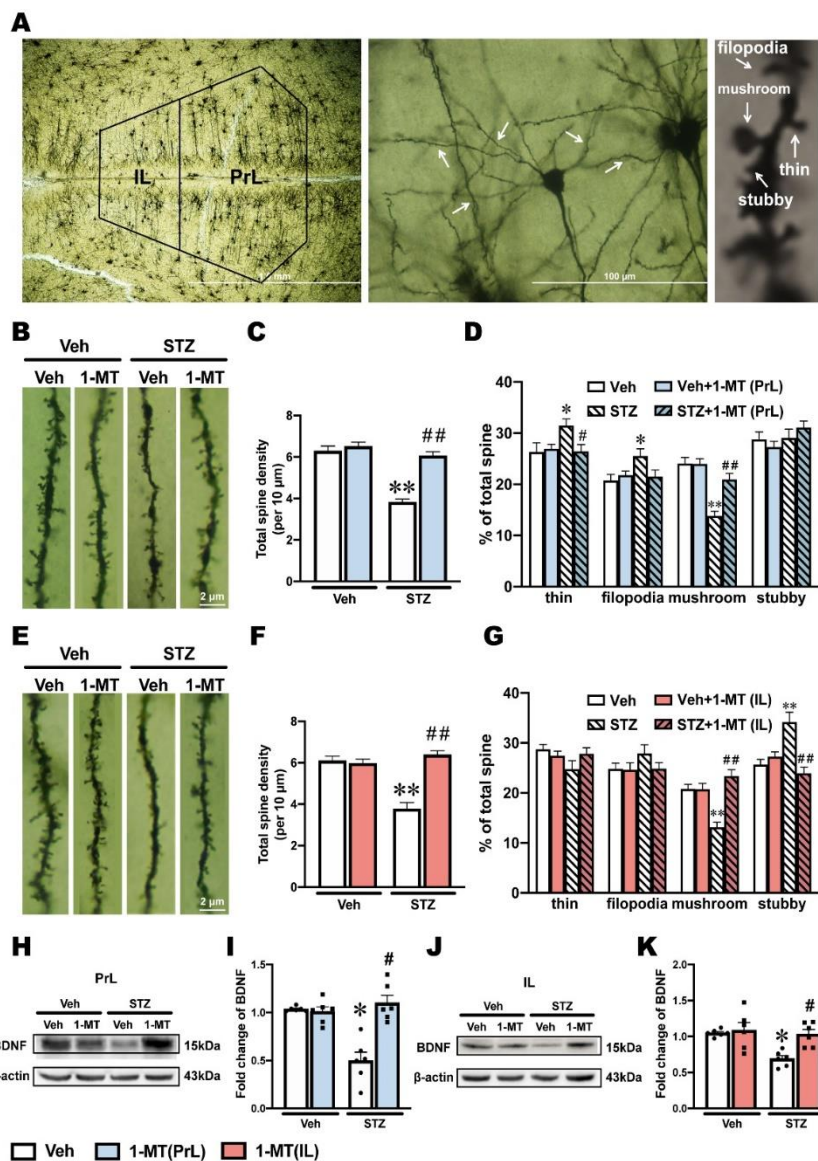


FIGURE 8: Intra-PrL or -IL administration of 1-MT improved synaptic deficits in the PrL and IL that were induced by ICV-STZ. **A)** Golgi staining of PrL and IL pyramidal neurons. **B)** Representative images of dendritic spines in the PrL. **C, D)** Total dendritic spine number and the proportion of each spine type were used to evaluate spine morphology alterations in the PrL. ($n = 18$ dendrites from 6 rats in each group). **E)** Representative images of dendritic

spines in the IL. **F, G**) Total dendritic spine number and the proportion of each spine type were used to evaluate spine morphology alterations in the IL. ($n = 18$ dendrites from 6 rats in each group). **H, I**) Western blots and quantification of BDNF in the PrL. **J, K**) Western blots and quantification of BDNF in the IL. β -actin was used as a quantitative loading control ($n = 6$). The data are expressed as individual values with means \pm SEM. * $p < 0.05$, ** $p < 0.01$ vs vehicle group; # $p < 0.05$, ## $p < 0.01$ vs ICV-STZ group; two-way ANOVA followed by tukey's multiple-comparison post hoc test.

3.7. Synaptic Plasticity was Impaired in Both the PrL and IL in ICV-STZ Rats and Reversed by 1-MT

Abnormal IDO-related Kyn metabolism occurring in glial cells can promote neurogenesis and neuroplasticity [46, 47]. In addition, depression is highly correlated with impaired neuroplasticity [48, 49]. In the present study, golgi staining was used to visually observe dendritic spines, which revealed changes in synaptic plasticity and function (Figure 8A).

In the PrL, ICV-STZ rats exhibited significant decreases in dendritic spine density and the proportion of mushroom spines, which were reversed by the intra-PrL injection of 1-MT (Figures 8B-8D). Additionally, the proportion of thin and filopodia spines in the PrL was significantly increased by ICV-STZ. The intra-PrL injection of 1-MT reversed the increase in thin spines, whereas the increase in filopodia spines was only slightly and not significantly blocked by 1-MT (Figure 8D).

In the IL, ICV-STZ significantly decreased dendritic spine density and the proportion of mushroom spines, which were reversed by the intra-IL injection of 1-MT (Figures 8E-8G). In contrast, the proportion of stubby spines in the IL was increased significantly by ICV-STZ, which was reversed by the intra-IL injection of 1-MT (Figure 8G). BDNF is a dimeric protein that is often used as an indicator of neuroplasticity. The expression of BDNF in the PrL and IL markedly decreased in ICV-STZ rats, and the intra-PrL and intra-IL administration of 1-MT reverse these ICV-STZ-induced decreases in BDNF levels (Figures 8H-8K).

4. Discussion

ICV-STZ is a classical model to simulate sporadic AD. In our previous study, ICV-STZ rats exhibited typical pathological changes that are similar to sAD in humans, such as the hyperphosphorylation of tau in the brain, and they progressively showed impairments in learning and cognition beginning on d 14 [50]. In the present study, we found no such pathological changes or learning and memory impairments on d 7 after ICV-STZ administration, but depression-like behaviors appeared. In addition, ICV-STZ rats showed both depression-like behavior and memory impairment on d 14, and their cognitive symptoms further worsened on d 21, but depression-like behaviors disappeared (Figure 2). Forsell *et al.* [51] indicated that depressive symptoms progressively worsen as AD develops from mild to moderate dementia but become less common with severe dementia. This was consistent with our observations in ICV-STZ rats, suggesting that the ICV-STZ model may be a valid animal model for studying early depression associated with sAD.

Kyn pathway is the main route for metabolism of the essential amino acid Trp and is recognized as a major pathway connecting multiple systems such as inflammation, immune response, neurotransmitter transmission and oxidative stress [52]. Various enzymes and metabolites

of the Kyn pathway are closely associated with neurological and psychiatric disorders [53]. Tryptophan 2,3-dioxygenase (TDO), IDO1 and IDO2 are the first rate-limiting enzymes in the Kyn pathway. It is generally accepted that TDO, which is predominantly located in the liver, is the main enzyme under physiological conditions and its expression is regulated mainly by systemic corticosteroids levels [54]. Growing evidence supports that the accelerated production of systemic and central Kyn associated with inflammation is largely dependent on IDO1, whereas the physiological function of the IDO2 and its role in disorders involving KP activity is currently unknown [54]. In the present study, we found that ICV-STZ activated IDO in some brain regions that are associated with emotion. Among them, PrL and IL draw our attention since the ratio of Kyn/Trp and IDO activity significantly increased, which implies IDO activated in these brain regions on d 7 when the rats exhibited depression-like behavior (Figure 3). IDO activation is associated with several neurological disorders, and the Kyn pathway abnormalities were also found in different models of AD [20, 55] and depression [56, 57]. Based on these studies, we hypothesized that the activation of IDO-related Kyn pathway in PrL and IL might underlie depression-like behavior in ICV-STZ rats. To confirm this hypothesis, we microinjected 1-MT, an IDO inhibitor, into PrL or IL to block Kyn metabolism. We found that intra-PrL or intra-IL injections of 1-MT decreased IDO activation and improved multiple depression-like behaviors in ICV-STZ rats (Figure 4). These results suggested that IDO in PrL or IL may play a key role in the regulation of depression-like behaviors in ICV-STZ rats.

A massive evidence suggests that neurological and neurodegenerative disorders emerge from abnormalities in astrocytes and microglia [18, 58]. In the central nervous system, glia responds positively to neuroinflammation via the regulation of IDO-related Kyn metabolic balance [59, 60]. Homeostatic imbalance in Kyn downstream metabolites was suggested to be regulated by microglia and astrocytes, which might be a prominent mechanism of depression-like behaviors after IDO activation [18]. Although no differences were observed in the structural distribution of glial cells in the PrL and IL [61, 62], they appear to play different roles in regulating depression-like behaviors by widespread mechanism, including synaptic plasticity [63], GABAergic networks [64] and astroglial glutamate transporters [65]. The present study showed that astrocytes in the PrL and microglia in the IL were involved in regulating depression-like behaviors in the ICV-STZ model (Figures 5 & 6). GFAP is an important component of the cytoskeleton in astrocytes. A consistent decrease in GFAP expression has been found in frontal cortex tissue from major depressive disorder patients, and there is evidence that decreased GFAP expression in corticolimbic regions may be a common neurobiological deficit associated depression [66]. GLAST and GLT-1 are the primary transporters responsible for synaptic glutamate uptake and play an important role in maintaining physiological functions of astrocytes [67]. In neuropsychiatric disorders and most notably depression, reduced GLAST and GLT-1 have been observed in many different brain regions [66, 67]. Our results showed a decrease in the number of GFAP-positive cells and the expression of

GFAP, GLAST and GLT-1 proteins in the PrL, indicating the deficits in astrocytes and astrocytic dysfunction. Three-dimensional reconstructions of astrocytes also showed a decrease in the surface area and branch complexity of astrocytes in the PrL, suggesting atrophy and degeneration of astrocytes. These abnormalities in astrocytes were alleviated by intra-PrL injection of 1-MT. However, in the IL, we did not observe significant abnormalities in astrocytes when ICV-STZ rats exhibit depression-like behaviors. Instead, abnormal activation in microglia might be an adverse consequence of IDO activation in the IL. The decrease of KA in the IL induced by ICV-STZ and the therapeutic effect of 1-MT were not observed in the IL, suggesting that the decreased KA levels in the IL may be attributable to Kyn being more metabolized into 3-HK under ICV-STZ, rather than ICV-STZ related astrocytic deficits. In addition, we also observed differences between these two subregions in the ICV-STZ model in terms of microglia. Iba1 is a microglia/macrophage-specific calcium-binding protein. Recent studies have confirmed that the increase in Iba1 expression in activated microglia is associated with tau pathology and neuronal apoptosis in AD mouse models [22, 68, 69]. Resting microglia are characterized by a small soma with multiple protrusions to sense changes in the surrounding environment. When activated, microglia take on a characteristic "amoeba-like" shape, as evidenced by retracted protrusions, enlarged soma, and decreased branches [19]. We found that ICV-STZ activated microglia in the IL, as evidenced by an increase in the number of Iba1-positive cells, Iba1 levels and pro-inflammatory cytokines (IL-1 β and IL-6), together with a concomitant decrease in terminal points and enlargement of the soma volume, all of which were restored by intra-IL injection of 1-MT. Intriguingly, we did not observe the similar activation of microglia and the therapeutic effect of 1-MT in the PrL.

In the present study, we found that ICV-STZ activated IDO in both the PrL and IL with a different response in glial (Figure 7). Basically, central KAT II is predominantly located in astrocytes and metabolites Kyn to KA, whereas KMO is majorly expressed in microglia and metabolites Kyn to 3-HK [70]. KA has been largely described as one of these neuroprotective metabolites capable of antagonizing NMDA receptor-mediated excitatory neurotoxicity and exert antioxidant effects [71]. Increasing KA levels prevented spatial memory deficits and synaptic loss in mouse model of AD [72]. In contrast with KA, 3-HK is recognized as a neurotoxicity factor causing radical-induced oxidative damage, mitochondrial dysfunction and cell death [73]. AD patients showed high levels of 3-HK in serum and hippocampus [74, 75]. Present study showed that ICV-STZ-induced depression-like behavior were paralleled by a decrease in KA in the PrL and IL, a decrease in KAT II expression in the PrL, and an increase in 3-HK and KMO expression in the IL. Taken together, these results reveal a glia regional specific response induced by ICV-STZ and, surprisingly, raise the possibility that although the kynurenine pathway is activated by ICV-STZ in both PrL and IL, the kynurenine pathway goes in different branches in two subregions.

Specifically, the neuroprotective branch is diminished in the PrL and the neurotoxic branch is enhanced in the IL, which may be involved in the development of ICV-STZ-induced depression-like behaviors. Additionally, the antidepressant effects of 1-MT in the PrL might occur through the normalization of astrocytic deficits and neuroprotective

branches, whereas the antidepressant effects of 1-MT in the IL might be at least partially mediated by local anti-inflammatory processes and the blockade of the neurotoxicity branches.

Studies in human and animals indicate that the central inflammatory response may be associated with a reduction of total volume of neuron, the shrinkage of dendrites, and the loss of dendritic spines in the mPFC [76, 77]. Some studies have shown that under conditions of chronic or acute stress, dendritic branches of neurons retract in the PrL [78] and IL [79]. Although glial cells in the PrL and IL regulate depression-like behaviors through different mechanisms, neurons in these two subregions exhibit similar morphological damage, such as a reduction of synaptic plasticity (Figure 8). In the present study, dendritic spine density, the proportion of mushroom-type spines, and BDNF levels in the PrL and IL significantly decreased in ICV-STZ rats. Mushroom-type spines are the main type of spine that is involved in the regulation of synaptic plasticity because it is more stable and has larger postsynaptic densities and contact areas than other spine types [80]. Notably, these two subregions differed with regard to alterations of the proportions of dendritic spine types in ICV-STZ rats. Increases in thin-type and filopodia-type spine proportions on dendrites were found in the PrL. In the IL, a larger proportion of stubby-type spines was mainly detected. These differences indicated that the deficient in the neuroprotective effects from astrocytes and the inflammatory stress from microglia induced different dynamic evolution in synaptic plasticity. Although 1-MT selectively restored distinct glial cell abnormalities in the PrL and IL, 1-MT administration significantly improved neuroplasticity and BDNF deficiency in both subregions, suggesting an additional antidepressant mechanism that is implicated in the structural remodeling of dendritic spines.

There is growing evidence indicates that conventional antidepressants cannot effectively ameliorate depressive symptoms in AD patients [1, 81], suggesting that depression accompanied by AD may have a different pathogenesis. According to our study, modulation of kynurenine pathway may be a more effective treatment strategy for AD associated depression. Although a clear explanation for the mechanism of sAD formation is still lacking, the ICV-STZ rodent model might make a valuable contribution to the field of sAD model research. It is necessary to further study whether this animal model can simulate clinical processes that are associated with sAD.

5. Conclusion

Overall, ICV-STZ induced depression-like behavior before cognitive impairment in rats. In ICV-STZ rats, IDO was activated in the PrL and IL, but the mechanisms that were involved in regulating depressive-like behaviors in these two subregions were different. The results provide clear evidence that exploring subregional mechanisms of the mPFC is important for further understanding the pathogenesis and treatment of depression. Selective inhibition of IDO reversed ICV-STZ-induced depression-like behaviors by ameliorating neuroprotective branch deficits in the PrL and inhibiting neurotoxic branch overactivation in the IL. These findings provide valuable information for further understanding the pathogenesis of depression, which may contribute to discovering novel treatment targets for depression, especially among the population who has a high risk of AD.

Availability of Data and Materials

The datasets used and/or analysed during the current study are available from the corresponding author on reasonable request.

Competing Interests

None.

Funding

This study was funded by grants from the National Natural Science Foundation of China (No. 82073829) and Pharmaceutical Innovation Varieties and Platform Cultivation Projects founded by Beijing Municipal Science & Technology Commission, Administrative Commission of Zhongguancun Science Park (No. Z221100007922035).

Author Contributions

YQ designed the experiment, performed the behavioral test and biochemical test, analysed experiment data, and was a major contributor in writing the manuscript. XH performed the biochemical experiment and analysed experiment data. HLZ collected the image of glia cells and analysed the morphological changes. NK investigated the background of the animal model and analysed the behavioral test. XC counted the number of immunofluorescence image and investigated the detail method of experiment. JKY performed the behavioral test and analysed the immobility time of forced swim test. YZ analysed the discrimination index of novel object recognition test. SYC provided the project administration and supervision, reviewed and edited the writing. YHZ provided the funding support, project administration and supervision, reviewed and edited the writing. All authors read and approved the final manuscript.

Acknowledgements

Not applicable.

Abbreviations

ICV-STZ: Intracerebroventricular Injection Of Streptozotocin
sAD: Sporadic Alzheimer's Disease
IDO: Indoleamine 2,3-Dioxygenase
PrL: Prelimbic Cortex
IL: Infralimbic Cortex
KAT II: Kynurenine Aminotransferase II
KMO: Kynurenine 3-Monooxygenase
AD: Alzheimer's Disease
Trp: Tryptophan
Kyn: Kynurenine
A β : Amyloid- β
KA: Kynurenic Acid
3-HK: 3-Hydroxy-Kynurenine
PFC: Prefrontal Cortex
mPFC: Medial Prefrontal Cortex
STZ: Streptozotocin
1-MT: 1-Methyl-DL-Tryptophan

FST: Forced Swim Test

SPT: Sucrose Preference Test

OFT: Open Field Test

NORT: Novel Object Recognition Test

NSFT: Novelty-Suppressed Feeding Test

5-HT: 5-Hydroxytryptamin

GFAP: Glial Fibrillary Acidic Protein

GLAST: Glutamate-Aspartate Transporter

GLT-1: Glutamate Transporter-1

Iba1: Ionized Calcium-Binding Adaptor Molecule-1

IL-1 β : Interleukin-1 beta

IL-6: Interleukin-6

TNF- α : Tumor Necrosis Factor Alpha

BDNF: Brain-Derived Neurotrophic Factor

REFERENCES

- [1] Anna D Burke, Danielle Goldfarb, Padmaja Bollam, et al. "Diagnosing and Treating Depression in Patients with Alzheimer's Disease." *Neurol Ther*, vol. 8, no. 2, pp. 325-350, 2019. View at: [Publisher Site](#) | [PubMed](#)
- [2] Tommaso Cassano, Silvio Calcagnini, Antonio Carbone, et al. "Pharmacological Treatment of Depression in Alzheimer's Disease: A Challenging Task." *Front Pharmacol*, vol. 27, no. 10, pp. 1067, 2019. View at: [Publisher Site](#) | [PubMed](#)
- [3] Shanna L Burke, Tamara Cadet, Amary Alcide, et al. "Psychosocial risk factors and Alzheimer's disease: the associative effect of depression, sleep disturbance, and anxiety." *Aging Ment Health*, vol. 22, no. 12, pp. 1577-1584, 2018. View at: [Publisher Site](#) | [PubMed](#)
- [4] Jennifer R Gatchel "Late-Life Depression and Alzheimer's Disease Pathology: An Ounce of Prevention, a Pound of Cure." *Am J Geriatr Psychiatry*, vol. 29, no. 5, pp. 458-461, 2021. View at: [Publisher Site](#) | [PubMed](#)
- [5] Vasiliki Orgeta, Naji Tabet, Ramin Nilforooshan, et al. "Efficacy of Antidepressants for Depression in Alzheimer's Disease: Systematic Review and Meta-Analysis." *J Alzheimers Dis*, vol. 58, no. 3, pp. 725-733, 2017. View at: [Publisher Site](#) | [PubMed](#)
- [6] Nunzio Pomara, John Sidtis "Possible therapeutic implication of Abeta disturbances in depression." *Int J Geriatr Psychiatry*, vol. 22, no. 9, pp. 931-932, 2007. View at: [Publisher Site](#) | [PubMed](#)
- [7] Jose A Soria Lopez, Hector M González, Gabriel C Léger "Alzheimer's disease." *Handb Clin Neurol*, vol. 167, pp. 231-255, 2019. View at: [Publisher Site](#) | [PubMed](#)
- [8] A Junod, A E Lambert, W Stauffacher, et al. "Diabetogenic action of streptozotocin: relationship of dose to metabolic response." *J Clin Invest*, vol. 48, no. 11, pp. 2129-2139, 1969. View at: [Publisher Site](#) | [PubMed](#)
- [9] Konstantinos Kalafatakis, Apostolos Zarros "Intracerebroventricular administration of streptozotocin as an experimental approach to Alzheimer's disease." *Int J Neurosci*, vol. 124, no. 12, pp. 944-946, 2014. View at: [Publisher Site](#) | [PubMed](#)
- [10] Mubeen A Ansari, Muddanna S Rao, Aishah Al-Jarallah, et al. "Early time course of oxidative stress in hippocampal synaptosomes and cognitive loss following impaired insulin signaling in rats: Development of sporadic Alzheimer's disease." *Brain Res*, vol. 1798, pp. 148134, 2023. View at: [Publisher Site](#) | [PubMed](#)

- [11] Paweł Grieb “Intracerebroventricular Streptozotocin Injections as a Model of Alzheimer's Disease: in Search of a Relevant Mechanism.” *Mol Neurobiol*, vol. 53, no. 3, pp. 1741-1752, 2016. View at: [Publisher Site](#) | [PubMed](#)
- [12] Anand Kamal Sachdeva, Anurag Kuhad, Kanwaljit Chopra “Naringin ameliorates memory deficits in experimental paradigm of Alzheimer's disease by attenuating mitochondrial dysfunction.” *Pharmacol Biochem Behav*, vol. 127, pp. 101-110, 2014. View at: [Publisher Site](#) | [PubMed](#)
- [13] Ansab Akhtar, Jatinder Dhaliwal, Sangeeta Pilkhwah Sah “7,8-Dihydroxyflavone improves cognitive functions in ICV-STZ rat model of sporadic Alzheimer's disease by reversing oxidative stress, mitochondrial dysfunction, and insulin resistance.” *Psychopharmacology (Berl)*, vol. 238, no. 7, pp. 1991-2009. View at: [Publisher Site](#) | [PubMed](#)
- [14] Shayan Amiri, Arya Haj-Mirzaian, Majid Momeny, et al. “Streptozotocin induced oxidative stress, innate immune system responses and behavioral abnormalities in male mice.” *Neuroscience*, vol. 340, pp. 373-383, 2017. View at: [Publisher Site](#) | [PubMed](#)
- [15] Suely Ribeiro Bampi, Angela Maria Casaril, Mariana G Fronza, et al. “The selenocompound 1-methyl-3-(phenylselenanyl)-1H-indole attenuates depression-like behavior, oxidative stress, and neuroinflammation in streptozotocin-treated mice.” *Brain Res Bull*, vol. 161, pp. 158-165, 2020. View at: [Publisher Site](#) | [PubMed](#)
- [16] Leandro Cattelan Souza, Cristiano R Jesse, Marcelo Gomes de Gomes, et al. “Intracerebroventricular Administration of Streptozotocin as an Experimental Approach to Depression: Evidence for the Involvement of Proinflammatory Cytokines and Indoleamine-2,3-Dioxygenase.” *Neurotox Res*, vol. 31, no. 4, pp. 464-477, 2017. View at: [Publisher Site](#) | [PubMed](#)
- [17] Jonathan Savitz “The kynurenine pathway: a finger in every pie.” *Mol Psychiatry*, vol. 25, no. 1, pp. 131-147, 2020. View at: [Publisher Site](#) | [PubMed](#)
- [18] Xue Tao, Mingzhu Yan, Lisha Wang, et al. “Homeostasis Imbalance of Microglia and Astrocytes Leads to Alteration in the Metabolites of the Kynurenine Pathway in LPS-Induced Depressive-Like Mice.” *Int J Mol Sci*, vol. 21, no. 4, pp. 1460, 2020. View at: [Publisher Site](#) | [PubMed](#)
- [19] Haixia Wang, Yi He, Zuoli Sun, et al. “Microglia in depression: an overview of microglia in the pathogenesis and treatment of depression.” *J Neuroinflammation*, vol. 19, no. 1, pp. 132, 2022. View at: [Publisher Site](#) | [PubMed](#)
- [20] Leandro Cattelan Souza, Cristiano R Jesse, Marcelo Gomes de Gomes, et al. “Activation of Brain Indoleamine-2,3-dioxygenase Contributes to Depressive-Like Behavior Induced by an Intracerebroventricular Injection of Streptozotocin in Mice.” *Neurochem Res*, vol. 42, no. 10, pp. 2982-2995, 2017. View at: [Publisher Site](#) | [PubMed](#)
- [21] Taysa B Bassani, Joelle M Turnes, Eric L R Moura, et al. “Effects of curcumin on short-term spatial and recognition memory, adult neurogenesis and neuroinflammation in a streptozotocin-induced rat model of dementia of Alzheimer's type.” *Behav Brain Res*, vol. 335, pp. 41-54, 2017. View at: [Publisher Site](#) | [PubMed](#)
- [22] Leonardo C Souza 1, Marcos K Andrade 2, Evellyn M Azevedo, et al. “Andrographolide Attenuates Short-Term Spatial and Recognition Memory Impairment and Neuroinflammation Induced by a Streptozotocin Rat Model of Alzheimer's Disease.” *Neurotox Res*, vol. 40, no. 5, pp. 1440-1454, 2022. View at: [Publisher Site](#) | [PubMed](#)
- [23] Cara L Wellman, Justin L Bollinger, Kelly M Moench, et al. “Effects of stress on the structure and function of the medial prefrontal cortex: Insights from animal models.” *Int Rev Neurobiol*, vol. 150, pp. 129-153, 2020. View at: [Publisher Site](#) | [PubMed](#)
- [24] Demetrio Sierra-Mercado, Nancy Padilla-Coreano, Gregory J Quirk “Dissociable roles of prelimbic and infralimbic cortices, ventral hippocampus, and basolateral amygdala in the expression and extinction of conditioned fear.” *Neuropsychopharmacology*, vol. 36, no. 2, pp. 529-538, 2011. View at: [Publisher Site](#) | [PubMed](#)
- [25] Christina B Shin, Taylor J Templeton, Alvin S Chiu, et al. “Endogenous glutamate within the prelimbic and infralimbic cortices regulates the incubation of cocaine-seeking in rats.” *Neuropharmacology*, vol. 128, pp. 293-300, 2018. View at: [Publisher Site](#) | [PubMed](#)
- [26] Satoshi Suzuki, Akiyoshi Saitoh, Masanori Ohashi, et al. “The infralimbic and prelimbic medial prefrontal cortices have differential functions in the expression of anxiety-like behaviors in mice.” *Behav Brain Res*, vol. 304, pp. 120-124, 2016. View at: [Publisher Site](#) | [PubMed](#)
- [27] M^a Neus Fullana, Ana Covelo, Analía Bortolozzi, et al. “In vivo knockdown of astroglial glutamate transporters GLT-1 and GLAST increases excitatory neurotransmission in mouse infralimbic cortex: Relevance for depressive-like phenotypes.” *Eur Neuropsychopharmacol*, vol. 29, no. 11, pp. 1288-1294, 2019. View at: [Publisher Site](#) | [PubMed](#)
- [28] Nathalie Percie du Sert, Viki Hurst, Amrita Ahluwalia, et al. “The ARRIVE guidelines 2.0: Updated guidelines for reporting animal research.” *Br J Pharmacol*, vol. 177, no. 16, pp. 3617-3624, 2020. View at: [Publisher Site](#) | [PubMed](#)
- [29] George Paxinos, Charles Watson, “The Rat Brain in Stereotaxic Coordinates.” Academic Press, San Diego, 1986.
- [30] Su-Ying Cui, Jin-Zhi Song, Xiang-Yu Cui, et al. “Intracerebroventricular streptozotocin-induced Alzheimer's disease-like sleep disorders in rats: Role of the GABAergic system in the parabrachial complex.” *CNS Neurosci Ther*, vol. 24, no. 12, pp. 1241-1252, 2018. View at: [Publisher Site](#) | [PubMed](#)
- [31] Hui-Ling Zhao, Su-Ying Cui, Yu Qin, et al. “Prophylactic effects of sporoderm-removed *Ganoderma lucidum* spores in a rat model of streptozotocin-induced sporadic Alzheimer's disease.” *J Ethnopharmacol*, vol. 269, pp. 113725, 2021. View at: [Publisher Site](#) | [PubMed](#)
- [32] Marcus A Lawson, Jennifer M Parrott, Robert H McCusker, et al. “Intracerebroventricular administration of lipopolysaccharide induces indoleamine-2,3-dioxygenase-dependent depression-like behaviors.” *J Neuroinflammation*, vol. 10, pp. 87, 2013. View at: [Publisher Site](#) | [PubMed](#)
- [33] J C O'Connor, M A Lawson, C André, et al. “Lipopolysaccharide-induced depressive-like behavior is mediated by indoleamine 2,3-dioxygenase activation in mice.” *Mol Psychiatry*, vol. 14, no. 5, pp. 511-522, 2009. View at: [Publisher Site](#) | [PubMed](#)
- [34] Hui Ding, Su-Ying Cui, Xiang-Yu Cui, et al. “Anti-stress effects of combined block of glucocorticoid and mineralocorticoid receptors in the paraventricular nucleus of the hypothalamus.” *Br J Pharmacol*, vol. 178, no. 18, pp. 3696-3707, 2021. View at: [Publisher Site](#) | [PubMed](#)
- [35] Hui Ye, Xiang-Yu Cui, Hui Ding, et al. “Melanin-Concentrating Hormone (MCH) and MCH-R1 in the Locus Coeruleus May Be Involved in the Regulation of Depressive-Like Behavior.” *Int J*

- Neuropsychopharmacol*, vol. 21, no. 12, pp. 1128-1137, 2018. View at: [Publisher Site](#) | [PubMed](#)
- [36] Meng-Ying Liu, Chun-Yu Yi, Li-Juan Zhu, et al. "Sucrose preference test for measurement of stress-induced anhedonia in mice." *Nat Protoc*, vol. 13, no. 7, pp. 1686-1698, 2018. View at: [Publisher Site](#) | [PubMed](#)
- [37] Lindsay M Lueptow "Novel Object Recognition Test for the Investigation of Learning and Memory in Mice." *J Vis Exp*, no. 126, pp. 55718, 2017. View at: [Publisher Site](#) | [PubMed](#)
- [38] Kenichi Fukumoto, Shigeyuki Chaki "Involvement of serotonergic system in the effect of a metabotropic glutamate 5 receptor antagonist in the novelty-suppressed feeding test." *J Pharmacol Sci*, vol. 127, no. 1, pp. 57-61, 2015. View at: [Publisher Site](#) | [PubMed](#)
- [39] Xue-Mei Han, Yan-Jie Qin, Ying Zhu, et al. "Development of an underivatized LC-MS/MS method for quantitation of 14 neurotransmitters in rat hippocampus, plasma and urine: Application to CUMS induced depression rats." *J Pharm Biomed Anal*, vol. 174, pp. 683-695, 2019. View at: [Publisher Site](#) | [PubMed](#)
- [40] Lunhao Chen, Yaling Hu, Siyuan Wang, et al. "mTOR-neuropeptide Y signaling sensitizes nociceptors to drive neuropathic pain." *JCI Insight*, vol. 7, no. 22, pp. e159247, 2022. View at: [Publisher Site](#) | [PubMed](#)
- [41] Masaki Kajimoto, Muhammad Nuri, Justin R Sleasman, et al. "Inhaled nitric oxide reduces injury and microglia activation in porcine hippocampus after deep hypothermic circulatory arrest." *J Thorac Cardiovasc Surg*, vol. 161, no. 6, pp. e485-e498, 2021. View at: [Publisher Site](#) | [PubMed](#)
- [42] C Tackenberg, A Ghori, R Brandt "Thin, stubby or mushroom: spine pathology in Alzheimer's disease." *Curr Alzheimer Res*, vol. 6, no. 3, pp. 261-268, 2009. View at: [Publisher Site](#) | [PubMed](#)
- [43] Debasis Nayak, Theodore L Roth, Dorian B McGavern "Microglia development and function." *Annu Rev Immunol*, vol. 32, pp. 367-402, 2014. View at: [Publisher Site](#) | [PubMed](#)
- [44] Andrés Vidal-Itriago, Rowan A W Radford, Jason A Aramideh, et al. "Microglia morphophysiological diversity and its implications for the CNS." *Front Immunol*, vol. 13, pp. 997786, 2022. View at: [Publisher Site](#) | [PubMed](#)
- [45] Hongye Liu, Lei Ding, Huifeng Zhang, et al. "The Metabolic Factor Kynurenic Acid of Kynurenine Pathway Predicts Major Depressive Disorder." *Front Psychiatry*, vol. 9, pp. 552, 2018. View at: [Publisher Site](#) | [PubMed](#)
- [46] Caroline M Forrest, Omari S Khalil, Mazura Pizar, et al. "Prenatal inhibition of the tryptophan-kynurenine pathway alters synaptic plasticity and protein expression in the rat hippocampus." *Brain Res*, vol. 1504, pp. 1-15, 2013. View at: [Publisher Site](#) | [PubMed](#)
- [47] Katherine O'Farrell, Eimear Fagan, Thomas J Connor, et al. "Inhibition of the kynurenine pathway protects against reactive microglial-associated reductions in the complexity of primary cortical neurons." *Eur J Pharmacol*, vol. 810, pp. 163-173, 2017. View at: [Publisher Site](#) | [PubMed](#)
- [48] Ronald S Duman, George K Aghajanian, Gerard Sanacora, et al. "Synaptic plasticity and depression: new insights from stress and rapid-acting antidepressants." *Nat Med*, vol. 22, no. 3, pp. 238-249, 2016. View at: [Publisher Site](#) | [PubMed](#)
- [49] J Blair Price, Carrie Bronars, Sophie Erhardt, et al. "Bioenergetics and synaptic plasticity as potential targets for individualizing treatment for depression." *Neurosci Biobehav Rev*, vol. 90, pp. 212-220, 2018. View at: [Publisher Site](#) | [PubMed](#)
- [50] Jin-Zhi Song, Su-Ying Cui, Xiang-Yu Cui, et al. "Dysfunction of GABAergic neurons in the parafacial zone mediates sleep disturbances in a streptozotocin-induced rat model of sporadic Alzheimer's disease." *Metab Brain Dis*, vol. 33, no. 1, pp. 127-137, 2018. View at: [Publisher Site](#) | [PubMed](#)
- [51] Y Forsell, A F Jorm, L Fratiglioni, et al. "Application of DSM-III-R criteria for major depressive episode to elderly subjects with and without dementia." *Am J Psychiatry*, vol. 150, no. 8, pp. 1199-1202, 1993. View at: [Publisher Site](#) | [PubMed](#)
- [52] Michael D Lovelace, Bianca Varney, Gayathri Sundaram, et al. "Recent evidence for an expanded role of the kynurenine pathway of tryptophan metabolism in neurological diseases." *Neuropharmacology*, vol. 112, no. Pt B, pp. 373-388, 2017. View at: [Publisher Site](#) | [PubMed](#)
- [53] Dan Li, Shuang Yu, Yu Long, et al. "Tryptophan metabolism: Mechanism-oriented therapy for neurological and psychiatric disorders." *Front Immunol*, vol. 13, pp. 985378, 2022. View at: [Publisher Site](#) | [PubMed](#)
- [54] Hidetsugu Fujigaki, Yasuko Yamamoto, Kuniaki Saito "L-Tryptophan-kynurenine pathway enzymes are therapeutic target for neuropsychiatric diseases: Focus on cell type differences." *Neuropharmacology*, vol. 112, no. Pt B, pp. 264-274, 2017. View at: [Publisher Site](#) | [PubMed](#)
- [55] Leandro Cattelan Souza, Cristiano R Jesse, Michelle S Antunes, et al. "Indoleamine-2,3-dioxygenase mediates neurobehavioral alterations induced by an intracerebroventricular injection of amyloid-beta1-42 peptide in mice." *Brain Behav Immun*, vol. 56, pp. 363-377, 2016. View at: [Publisher Site](#) | [PubMed](#)
- [56] Yuanyuan Deng, Manfei Zhou, Junfeng Wang, et al. "Involvement of the microbiota-gut-brain axis in chronic restraint stress: disturbances of the kynurenine metabolic pathway in both the gut and brain." *Gut Microbes*, vol. 13, no. 1, pp. 1-16, 2021. View at: [Publisher Site](#) | [PubMed](#)
- [57] Juncai Pu, Yiyun Liu, Siwen Gui, et al. "Metabolomic changes in animal models of depression: a systematic analysis." *Mol Psychiatry*, vol. 26, no. 12, pp. 7328-7336, 2021. View at: [Publisher Site](#) | [PubMed](#)
- [58] Linglin Yang, Yunxiang Zhou 2, Honglei Jia, et al. "Affective Immunology: The Crosstalk Between Microglia and Astrocytes Plays Key Role?" *Front Immunol*, vol. 11, pp. 1818, 2020. View at: [Publisher Site](#) | [PubMed](#)
- [59] Livia Dezsi, Bernadett Tuka, Diana Martos, et al. "Alzheimer's disease, astrocytes and kynurenines." *Curr Alzheimer Res*, vol. 12, no. 5, pp. 462-480, 2015. View at: [Publisher Site](#) | [PubMed](#)
- [60] Allison M Garrison, Jennifer M Parrott, Arnulfo Tuñon, et al. "Kynurenine pathway metabolic balance influences microglia activity: Targeting kynurenine monooxygenase to dampen neuroinflammation." *Psychoneuroendocrinology*, vol. 94, pp. 1-10, 2018. View at: [Publisher Site](#) | [PubMed](#)
- [61] María Banqueri, Marta Méndez, Eneritz Gómez-Lázaro, et al. "Early life stress by repeated maternal separation induces long-term neuroinflammatory response in glial cells of male rats." *Stress*, vol. 22, no. 5, pp. 563-570, 2019. View at: [Publisher Site](#) | [PubMed](#)
- [62] R-D Gosselin, S Gibney, D O'Malley, et al. "Region specific decrease in glial fibrillary acidic protein immunoreactivity in the brain of a rat model of depression." *Neuroscience*, vol. 159, no. 2, pp. 915-925, 2009. View at: [Publisher Site](#) | [PubMed](#)
- [63] Emilio Garro-Martínez, Maria Neus Fullana, Eva Florensa-Zanuy, et al. "mTOR Knockdown in the Infralimbic Cortex Evokes A

- Depressive-like State in Mouse.” *Int J Mol Sci*, vol. 22, no. 16, pp. 8671, 2021. View at: [Publisher Site](#) | [PubMed](#)
- [64] Boldizsár Czéh, Irina Vardya, Zsófia Varga, et al. “Long-Term Stress Disrupts the Structural and Functional Integrity of GABAergic Neuronal Networks in the Medial Prefrontal Cortex of Rats.” *Front Cell Neurosci*, vol. 12, pp. 148, 2018. View at: [Publisher Site](#) | [PubMed](#)
- [65] M Neus Fullana, Esther Ruiz-Bronchal, Albert Ferrés-Coy, et al. “Regionally selective knockdown of astroglial glutamate transporters in infralimbic cortex induces a depressive phenotype in mice.” *Glia*, vol. 67, no. 6, pp. 1122-1137, 2019. View at: [Publisher Site](#) | [PubMed](#)
- [66] Ronald Kim, Kati L Healey, Marian T Sepulveda-Orengo, et al. “Astroglial correlates of neuropsychiatric disease: From astrocytopathy to astrogliosis.” *Prog Neuropsychopharmacol Biol Psychiatry*, vol. 87, no. Pt A, pp. 126-146, 2018. View at: [Publisher Site](#) | [PubMed](#)
- [67] Edward Pajarillo, Asha Rizor, Jayden Lee, et al. “The role of astrocytic glutamate transporters GLT-1 and GLAST in neurological disorders: Potential targets for neurotherapeutics.” *Neuropharmacology*, vol. 161, pp. 107559, 2019. View at: [Publisher Site](#) | [PubMed](#)
- [68] Elham Nasiri, Roman Sankowski, Henriette Dietrich, et al. “Key role of MIF-related neuroinflammation in neurodegeneration and cognitive impairment in Alzheimer's disease.” *Mol Med*, vol. 26, no. 1, pp. 34, 2020. View at: [Publisher Site](#) | [PubMed](#)
- [69] Haihao Zhu, Xiehua Xue, Erming Wang, et al. “Amylin receptor ligands reduce the pathological cascade of Alzheimer's disease.” *Neuropharmacology*, vol. 119, pp. 170-181, 2017. View at: [Publisher Site](#) | [PubMed](#)
- [70] Radhika Sharma, Karan Razdan, Yashika Bansal, et al. “Rollercoaster ride of kynurenines: steering the wheel towards neuroprotection in Alzheimer's disease.” *Expert Opin Ther Targets*, vol. 22, no. 10, pp. 849-867, 2018. View at: [Publisher Site](#) | [PubMed](#)
- [71] R Lugo-Huitrón, T Blanco-Ayala, P Ugalde-Muñiz, et al. “On the antioxidant properties of kynurenic acid: free radical scavenging activity and inhibition of oxidative stress.” *Neurotoxicol Teratol*, vol. 33, no. 5, pp. 538-547, 2011. View at: [Publisher Site](#) | [PubMed](#)
- [72] Daniel Zwilling, Shao-Yi Huang, Korrapati V Sathyasaikumar, et al. “Kynurenine 3-monooxygenase inhibition in blood ameliorates neurodegeneration.” *Cell*, vol. 145, no. 6, pp. 863-874, 2011. View at: [Publisher Site](#) | [PubMed](#)
- [73] Ana Laura Colín-González, Perla D Maldonado, Abel Santamaría, et al. “3-Hydroxykynurenine: an intriguing molecule exerting dual actions in the central nervous system.” *Neurotoxicology*, vol. 34, pp. 189-204, 2013. View at: [Publisher Site](#) | [PubMed](#)
- [74] David J Bonda, Maneesh Mailankot, Jeremy G Stone, et al. “Indoleamine 2,3-dioxygenase and 3-hydroxykynurenine modifications are found in the neuropathology of Alzheimer's disease.” *Redox Rep*, vol. 15, no. 4, pp. 161-168, 2010. View at: [Publisher Site](#) | [PubMed](#)
- [75] Markus J Schwarz, Gilles J Guillemin, Stefan J Teipel, et al. “Increased 3-hydroxykynurenine serum concentrations differentiate Alzheimer's disease patients from controls.” *Eur Arch Psychiatry Clin Neurosci*, vol. 263, no. 4, pp. 345-352, 2013. View at: [Publisher Site](#) | [PubMed](#)
- [76] Cuiqin Fan, Qiqi Song, Peng Wang, et al. “Curcumin Protects Against Chronic Stress-induced Dysregulation of Neuroplasticity and Depression-like Behaviors via Suppressing IL-1beta Pathway in Rats.” *Neuroscience*, vol. 392, pp. 92-106, 2018. View at: [Publisher Site](#) | [PubMed](#)
- [77] Timothy B Meier, Wayne C Drevets, Brent E Wurfel, et al. “Relationship between neurotoxic kynurenine metabolites and reductions in right medial prefrontal cortical thickness in major depressive disorder.” *Brain Behav Immun*, vol. 53, pp. 39-48, 2016. View at: [Publisher Site](#) | [PubMed](#)
- [78] Kelly M Moench, Cara L Wellman “Differential dendritic remodeling in prefrontal cortex of male and female rats during recovery from chronic stress.” *Neuroscience*, vol. 357, pp. 145-159, 2017. View at: [Publisher Site](#) | [PubMed](#)
- [79] Kelly M Moench, Mouna Maroun, Alexandra Kavushansky, et al. “Alterations in neuronal morphology in infralimbic cortex predict resistance to fear extinction following acute stress.” *Neurobiol Stress*, vol. 3, pp. 23-33, 2015. View at: [Publisher Site](#) | [PubMed](#)
- [80] Martin S Helm, Tal M Dankovich, Sunit Mandad, et al. “A large-scale nanoscopy and biochemistry analysis of postsynaptic dendritic spines.” *Nat Neurosci*, vol. 24, no. 8, pp. 1151-1162, 2021. View at: [Publisher Site](#) | [PubMed](#)
- [81] Yanhong He, Hao Li, Jinbo Huang, et al. “Efficacy of antidepressant drugs in the treatment of depression in Alzheimer disease patients: A systematic review and network meta-analysis.” *J Psychopharmacol*, vol. 35, no. 8, pp. 901-909, 2021. View at: [Publisher Site](#) | [PubMed](#)